Acta Pharmaceutica Sinica B 2023;13(12):4856–4874

Chinese Pharmaceutical Association
Institute of Materia Medica, Chinese Academy of Medical Sciences

Acta Pharmaceutica Sinica B

www.elsevier.com/locate/apsb
www.sciencedirect.com

ORIGINAL ARTICLE

Immunogenicity of mucosal COVID-19 vaccine candidates based on the highly attenuated vesicular stomatitis virus vector (VSV_{MT}) in golden syrian hamster

Yong Ke[a,†], En Zhang[b,c,†], Jianming Guo[b,c], Xiaoxiao Zhang[b,c], Lei Wang[a], Duo Chen[b,c], Xinkui Fang[b], Jianwei Zhu[a], Feng Li[d,*], Tao Sun[b,c,*], Baohong Zhang[a,*]

[a]*Engineering Research Center of Cell & Therapeutic Antibody, Ministry of Education, School of Pharmacy, Shanghai Jiao Tong University, Shanghai 200240, China*
[b]*School of Agriculture and Biology, Shanghai Jiao Tong University, Shanghai 200240, China*
[c]*Shanghai Municipal Veterinary Key Laboratory, Shanghai 200240, China*
[d]*Shanghai Public Health Clinical Center, Fudan Univeristy, Shanghai 201508, China*

Received 2 April 2023; received in revised form 10 July 2023; accepted 9 August 2023

KEY WORDS

COVID-19;
Vesicular stomatitis virus;
Matrix protein mutant;
Mucosal Vaccine;
Spike protein;
Variants of concerns;
Intranasal inoculation;
Cellular immunity

Abstract COVID-19 is caused by coronavirus SARS-CoV-2. Current systemic vaccines generally provide limited protection against viral replication and shedding within the airway. Recombinant VSV (rVSV) is an effective vector which inducing potent and comprehensive immunities. Currently, there are two clinical trials investigating COVID-19 vaccines based on VSV vectors. These vaccines were developed with spike protein of WA1 which administrated intramuscularly. Although intranasal route is ideal for activating mucosal immunity with VSV vector, safety is of concern. Thus, a highly attenuated rVSV with three amino acids mutations in matrix protein (VSV_{MT}) was developed to construct safe mucosal vaccines against multiple SARS-CoV-2 variants of concern. It demonstrated that spike protein mutant lacking 21 amino acids in its cytoplasmic domain could rescue rVSV efficiently. VSV_{MT} indicated improved safeness compared with wild-type VSV as the vector encoding SARS-CoV-2 spike protein. With a single-dosed intranasal inoculation of $rVSV_{\Delta GMT}$-$S_{\Delta 21}$, potent SARS-CoV-2 specific neutralization antibodies could be stimulated in animals, particularly in term of mucosal and cellular immunity. Strikingly, the chimeric VSV encoding $S_{\Delta 21}$ of Delta-variant can induce more potent immune responses

*Corresponding authors.
E-mail addresses: lifeng30286@shaphc.org (Feng Li), tao.sun@sjtu.edu.cn (Tao Sun), bhzhang@sjtu.edu.cn (Baohong Zhang).
[†]These authors made equal contributions to this work.
Peer review under the responsibility of Chinese Pharmaceutical Association and Institute of Materia Medica, Chinese Academy of Medical Sciences.

https://doi.org/10.1016/j.apsb.2023.08.023

compared with those encoding $S_{\Delta 21}$ of Omicron- or WA1-strain. VSV_{MT} is a promising platform to develop a mucosal vaccine for countering COVID-19.

1. Introduction

Since the outbreak of COVID-19, it has resulted in the loss of over 6 million people[1]. The COVID-19 pandemic is caused by SARS-CoV-2, a human coronavirus that primarily infects and transmits through the respiratory tract. SARS-CoV-2 gains enter into host cells by utilizing angiotensin-converting enzyme II (ACE2) as the receptor[2,3]. Its spike protein is in charge of the attachment with ACE2, triggering the production of neutralizing protective antibodies, and is considered to be the primary antigens for current vaccine development[4,5].

Vaccines have proved to be the most effective method for controlling the epidemic of COVID-19. Varieties of platforms have been utilized to deliver the S protein of parental strain, including inactivated virion, lipid nanoparticle encapsulated mRNA and viral-vectored vaccines[6–9]. To date, the emergence of at least five variants of concerns (VOCs), particularly the Delta and Omicron, has raised significant attention due to their virulence and transmissibility[10]. Of note, both have the ability to evade the protection provided by current vaccines[11,12]. In addition to the challenge of existing vaccines due to emerging VOCs, their inability to effectively elicit mucosal immunity against SARS-CoV-2 infection may also be another key reason[11,13]. Systemic respiratory vaccines typically provide limited protection against SARS-CoV-2, which requires a local mucosal secretory IgA response within the airway[14].

Vesicular stomatitis virus (VSV) has emerged as a distinguished vaccine vector against microbial pathogens. The advantages of recombinant VSV (rVSV) lie in its robust growth in approved mammalian cell lines and its capability to elicit potent cellular and humoral immune responses[15]. In 2019, a VSV-based vaccine (known as Ervebo) against Ebola Virus has been approved by FDA[16]. Currently, there have been at least two clinical trials involved in the evaluation of COVID-19 vaccines developed with VSV vector[17,18]. Of note, there is currently no available report regarding VSV-based vaccine candidates specifically targeting the Delta and Omicron variants. VSV vector-based vaccine delivered by nasal route is ideal for immunization. However, the main obstacle to its application is the concern of safety, such as potential neurotoxicity[19–21]. Previously, a mutant VSV(VSV_{MT}) with triple mutations (S226R, V221F, and ΔM51) occurring at its matrix protein (M) was constructed by the lab, which demonstrated a significant attenuation compared to wild-type VSV and $VSV_{\Delta M51}$ with a single amino acid deletion in M protein. The attenuation of VSV_{MT} lies in its significantly diminished ability to inhibit type I interferon signaling and host gene expression[22]. In our study, S protein mutant of SARS-CoV-2 with 21 amino acids deleted in the cytoplasmic domain ($S_{\Delta 21}$) was capable of incorporating into VSV particles with high efficiency. Thus, we rescued a series of chimeric $rVSV_{MT}$ encoding $S_{\Delta 21}$ mutant of the parental strain of WA1, Delta, and Omicron variants, with VSV glycoprotein (G) deleted. Their immunogenicity was evaluated and compared in the animal model, including the golden syrian hamster and hACE2 mouse, *via* mucosal routes of intranasal (IN) and *per oral* (*PO*) administration. Importantly, SARS-CoV-2 specific humoral, mucosal as well as T cell-mediated immune responses can be effectively and comprehensively stimulated with one shot of the intranasal administration. Strikingly, the candidate vaccine encoding Delta strain S protein exhibited more efficient replication *in vitro* and stimulate more potent immune responses *in vivo,* particularly when administered *via* the intranasal route. The study demonstrated that VSV_{MT} encoding Spike protein can induce potent immune responses *in vivo.* Therefore, VSV_{MT} can be the promising platform to develop novel mucosal vaccines for countering COVID-19.

2. Materials and methods

2.1. Cell lines and viruses

Huh-7 cells (NIBIO, China), baby hamster kidney cells (BHK-21) (ATCC) and African green monkey cells (VeroE6) (ATCC) were cultured in 10% fetal bovine serum (Gibco) DMEM medium. Cells were grown in 5% CO_2 37 °C humidified air. Replication of incompetent virus G-$rVSV_{\Delta G}$-GFP was made and kept in the lab.

2.2. Plasmid construction

To characterize the optimal cytoplasmic tail of the SARS-CoV-2 spike protein for constructing retargeting VSV virus, we initially constructed plasmids encoding the spike protein gene as well as its mutants with sequential deletions of carboxyl-terminal amino acids. The human codon-optimized sequences of the S protein gene of prototype-WA1 and VOCs (Delta and Omicron) were utilized (GenBank: ON872488.1, MW408785.1, and OW996240.1). S_{FL}, $S_{\Delta 19}$, $S_{\Delta 20}$, $S_{\Delta 21}$, $S_{\Delta 22}$, $S_{\Delta 23}$, $S_{\Delta 24}$, $S_{\Delta 25}$ and $S_{\Delta 26}$ represented the full-length Spike protein or Spike corresponding mutants with 19−26 amino acids truncated from the cytoplasmic tail. The PCR primers were shown in Supporting Information Table S1. The mutated genes were inserted into the eukaryotic expression plasmid pIRES. These plasmids were named pIRES-$S_{\Delta 19-26}$ or -S_{FL} (Table S1).

2.3. Flow cytometry

HEK293T cells were transfected with pIRES-$S_{\Delta 19-26}$ or -S_{FL} through Lipofectamine 2000 (Thermo Fisher). After 24 h, the transfected cells were assessed with rabbit anti-spike protein polyclonal Ab (Sino Biological). After incubation for 30 min, the cells were washed with DPBS, and stained with goat anti-rabbit IgG conjugated with Alexa Fluor 488. S protein expression levels were analyzed by flow cytometry (BD).

2.4. Recovery of replication-defective spike-rVSV$_{\Delta G}$-GFP

The replication-incompetent VSV particles pseudotyped with SARS-CoV-2 spike protein mutants were constructed as described previously[23]. Briefly, the recombinant plasmids pIRES-S_{FL} or pIRES-$S_{\Delta 19}$−$S_{\Delta 26}$ were transfected into HEK293T cells, with transfection occurring 24 h prior to infection with G-rVSV$_{\Delta G}$-GFP at a MOI of 1. After 24 h, the pseudotyped VSV particles, namely S_{FL}-rVSV$_{\Delta G}$-GFP or $S_{\Delta 19-26}$-rVSV$_{\Delta G}$-GFP, were harvested from the cell culture supernatants and subsequently used to infect hACE2-293T cells. The number of infected cells was quantified, enabling the determination of the infective units (IU) of the VSV pseudotypes.

2.5. Recovery of replication-competent chimeric rVSV encoding spike protein

A mutated spike protein gene with optimal cytoplasmic tail ($S_{\Delta 21}$) was cloned between MluI and XhoI restriction sites of pVSV$_{MT}$-GFP or pVSV-GFP plasmid to replace the G protein gene of VSV. The above plasmids were constructed and kept in the lab. The recovery of the rVSV$_{\Delta GMT}$-$S_{\Delta 21}$ (WA1, Delta, and Omicron) or rVSV$_{\Delta GMT}$-$S_{\Delta 21}$ viruses was carried out by Fang et al.[22]. Briefly, BHK21 cells were infected with recombinant vaccinia virus (vTF7-3) for an hour. Subsequently, these cells were co-transfected with plasmid pVSV$_{\Delta GMT}$-$S_{\Delta 21}$-GFP or pVSV$_{\Delta G}$-$S_{\Delta 21}$-GFP together with four helper plasmids (pBS-G, L, P, and N). After 48 h, the culture supernatants were collected, filtered through the 0.2 μm membrane and used to infect BHK21. The cells were observed daily until the typical cytopathic effect (CPE) appeared, and the culture supernatants were collected. The rescued viruses were initially amplified in BHK-21 cells transfected with pMD2G plasmid. Subsequently, the rVSVs were plaque-purified and expanded in Vero E6 cells.

2.6. Virion ultracentrifugation purification and negative staining

The chimeric VSVs expressing SARS-CoV2 spike protein were amplified in VeroE6 cells. The supernatants were collected and centrifuged at 780 × *g* for 30 min to remove debris and then the supernatants were filtered with a 0.45 μm filter. Samples were ultracentrifuged through a 20% (*w*/*w*) sucrose cushion at 90,000 × *g* for 1.5 h at 4 °C. The pelleted virions were then resuspended in DPBS and analyzed by SDS-PAGE followed by a silver staining kit (Beyotime).

Negative staining was performed to observe the intact morphology of the ultracentrifugation-purified rVSV$_{\Delta GMT}$-$S_{\Delta 21}$ virions. Briefly, virions were adsorbed to Formvar-coated copper mesh grids, negatively stained with 2% phosphotungstic acid solution and air dried. Digital images of virions were captured with an electron microscope (HITACHI 7800).

2.7. Genetic stability of M gene in VSV$_{MT}$ vector

The M gene with triple mutations plays a key role in the attenuation of the VSV$_{MT}$ vector. As the classical protocol to study the genetic stability of the viral vector, analysis including viral stock passaging, plaques purification, gene amplification as well as sequencing were performed as described[24]. In short, the Master Seed Viruses (MSV) of each rVSV$_{\Delta GMT}$-$S_{\Delta 21}$ was serially passaged for up to 10 passages in the VeroE6 production cell line. Virus infection was conducted using a multiplicity of infection (MOI) of 0.01, and the infected cells were incubated for 2 days. Afterward, the virus-containing supernatant was harvested and frozen at −80 °C for the next passaging round. The 5th and 10th passages for each virus were plaque purified. At least 10 viral plaques were randomly selected from each stock[24]. Viral RNA was extracted and the M protein gene was amplified after reverse transcription and sequenced. VSV-M gene PCR primers are as follows, forward: 5′-agaaattagggatcgcacca-3′; reverse: 5′-ctcca-gatgccttttctcg-3′.

2.8. Neutralization assay

Sera from the experimental animals were heat-treated at 56 °C for half an hour before antibody detection, and then serially diluted at a two-fold starting at 1:10 with DMEM. The bronchoalveolar lavage fluid (BALF) was also serially diluted two-fold starting at 1:2. To determine neutralizing antibody titers, 50 μL of the diluted sera or BALF samples were mixed with 50 μL DMEM containing 100 PFU of the corresponding VSV$_{\Delta GMT}$-$S_{\Delta 21}$-GFP virus encoding $S_{\Delta 21}$ of WA1, Delta or Omicron, respectively. The mixture was incubated at 37 °C for 1 h, then added to VeroE6 cells cultured in 96-well plates. One hour later, the cells were rinsed three times with DPBS and supplemented with DMEM media containing 2% FBS. At 24 h post-inoculation (h.p.i), the neutralization titers were calculated by observation under a fluorescence microscope. The titers were recorded as the reciprocal of the highest antibody dilution, which gave a 100% inhibition of the cytopathic effect[25,26]. The neutralization curves are fitted by four-parameter nonlinear regression using GraphPad Prism 8.

Dilutions of the purified monoclonal antibodies 2G1, REGN10987, and 8G3 were pre-incubated with Spike-rVSV$_{\Delta G}$-GFP pseudotyped with WA1, Delta or Omicron S protein for 1 h at 37 °C and then infected hACE2-293T cells. IC_{50} values of the antibodies were calculated as the reciprocal of their dilution fold, which caused a 50% reduction of the GFP^-positive cells at 24 h.p.i..

2.9. ELISPOT assay

Splenectomies were performed on human ACE2 transgenic mice that were immunized with various rVSV$_{\Delta GMT}$-$S_{\Delta 21}$ viruses. The mice were sacrificed at 0, 7 or 14 days post-immunization. After anesthesia, the whole spleen tissue was taken from mice, washed with sterile PBS, and then finely minced with sterile scissors. After homogenization, splenocytes were transferred to 50-mL conical tubes and centrifuged at 300 × *g* for 5 min. The pellets were resuspended in PBS. The cell suspension was poured through a sterile cell container with a 40 μm pore diameter to remove any large debris. Murine lymphocytes were isolated following the manufacturer's protocol (Solarbio). The isolated cells were then resuspended in 1 mL RPMI-1640 containing 10% FBS and counted. The ELISPOT analysis was carried out according to the manufacturer's protocol (Mabtech). Briefly, harvested cells from each mouse were seeded in triplicate at 3 × 10^5/well into 96-well plates precoated with IFN-γ mAb. Cells were pulsed with a 2 μg/mL peptide pool of SARS-CoV-2 spike protein PP003 (SinoBiological) at 37 °C in the CO_2 incubator. In addition, cells were plated as mock (nonpulsed) controls for each mouse group. After 20 h of incubation, the cell medium was removed, and plates

were washed extensively with PBS-0.5% FCS. Subsequently, each well was treated with 0.5 μg/mL of biotin-labeled anti-IFN-γ mAb. Following a 90-min incubation at room temperature and additional washes in PBS-0.5% FCS, 100 μL of 0.2 μg/mL streptavidin-alkaline phosphatase was added to each well. The wells were incubated for 1 h at room temperature and washed. The ready-to-use substrate solution (BCIP/NBT-plus) was added at 100 μL/well. After spot development, the plates were washed extensively with tap water. The plates were dried, and spots were quantified. The number of background ELISPOTS from mock wells were subtracted from the experimental groups. The results are presented as mean ELISPOTS per million cells ± standard deviations for each group ($n = 3$).

2.10. Real-time RT-PCR

Total RNA was extracted from homogenized animal tissues according to the manufacturer's instructions (Thermo Fisher). Briefly, 750 μL Trizol reagent was mixed with 250 μL supernatants from the homogenized tissues. After incubation for 5 min, 200 μL trichloromethane was added to the mixture and vortexed for 15 s. The mixture was centrifuged for 15 min at 11,000 × *g*, and 300 μL supernatants were collected and mixed with 300 μL isopropanol. The mixture was kept under −20 °C for 2 h. After centrifuging for 15 min at 11,000 × *g*, the pellet was washed with 75% ethyl alcohol. After centrifugation, the RNA was dissolved in DEPC-treated water. Viral cDNA was reverse transcribed using the First Strand RevertAid cDNA Synthesis Kit (Thermo Fisher). Real-time q-PCR was conducted with Premix Pro Taq HS qPCR SYBR Green II Kit (Accurate Biology). The primers used to detect VSV-N gene were as follows: forward: 5′-TGATCGACTTTGGATTGTCTTCTAA-3′, reverse: 5′-TCTGGTGGATCTGAGCAGAAGAG-3′.

2.11. Western blotting

VeroE6 was infected with various $rVSV_{\Delta GMT}$-$S_{\Delta 21}$ viruses at MOI of 1. At 24 h.p.i., the cell lysates were prepared using 5 × SDS-PAGE loading buffer with 1% PMSF and then centrifuged at 15,700 × *g* at 4 °C for 15 min. Cellular lysates were separated at 110 V for about 1 h and then transferred onto the PVDF membrane. Rabbit anti-spike antibody (SinoBiological) or mouse VSV convalescent serum were incubated with the PVDF membrane at 4 °C for 12 h. After three washes, goat anti-rabbit or anti-mouse IgG antibodies which were conjugated with HPR were incubated with the PVDF membrane at room temperature for 1 h. After washing with PBST three times, the bands on the PVDF membrane were identified with ECL reagent.

2.12. One-step growth curve

One-step growth curves were established in VeroE6 cells. Briefly, various $rVSV_{\Delta GMT}$-$S_{\Delta 21}$ viruses were inoculated into VeroE6 at an MOI of 3 and cultured in 12-well plates. The inoculum was removed and the cells were washed with DPBS after 1 h, followed by the addition of 2% fetal bovine serum DMEM media to the cells. Triplicate samples were collected at 4, 8, 12, 24 and 48 h.p.i., respectively, with viral titers identified by plaque-assays.

2.13. Animal experiments

Specific-pathogen-free (SPF) female LVG golden syrian hamsters (∼90 g) from Charles Rivers company were used to assess the safety of VSV_{MT} in contrast to wild-type VSV as the vector encoding spike protein. As shown in Table 1, hamsters were randomly felled into 5 groups of three animals each: hamsters were inoculated with 5×10^5 or 5×10^6 PFU $rVSV_{\Delta GMT}$-Delta or $rVSV_{\Delta G}$-Delta *via* IN route in 50 μL PBS, with PBS as the control. Blood specimens were gathered on Days 0, 3, 7, 14, 21, and 28 post-inoculation. On Day 28, the animals were euthanized, and their organs including spleen, lung, and testis were collected. In addition, bronchoalveolar lavage fluid (BALF) was collected through 1 mL PBS. All samples were stored at −80 °C.

Immunogenicity of COVID-19 vaccine candidates developed with live $rVSV_{MT}$ as the vector was evaluated in two different animal models, which were golden syrian hamsters and human ACE2 transgenic mice. As shown in Table 2, 21 groups of specific-pathogen-free (SPF) female LVG golden syrian hamsters were inoculated with 10^5 or 10^6 PFU $rVSV_{\Delta GMT}$-$S_{\Delta 21}$ *via* the IN, IM, and *PO* route in 50 μL PBS, with the PBS as control. Sera specimens were gathered on Days 7 and 28 post-vaccination. The animals were euthanized on Day 28; organs including the lung and brain were gathered followed by the store at −80 °C; bronchoalveolar lavage fluid (BALF) was collected through 1 mL PBS and stored at −80 °C for subsequent tests.

Human ACE2 transgenic mice were made by microinjection of DNA into zygotic pronuclei. As shown in Table 2, the transgenic mice were randomly divided into 12 groups of three animals: hACE2-mouse were inoculated with 10^6 PFU $rVSV_{MT}$-$S_{\Delta 21}$ *via* the IN, IM, and *PO* route in 50 μL PBS. All animals were inoculated on Day 0. Blood specimens were collected on Days 0, 7, and 28 until post-vaccination. The animals were euthanized on Day 28, and organs of the lungs and bronchoalveolar lavage fluid (BALF) were gathered in 1 mL PBS.

To test the cellular immunity induced by various $VSV_{\Delta GMT}$-$S_{\Delta 21}$ *via* mucosal route, hACE2 mice were grouped as shown in Table 3, which were vaccinated with 10^5 or 10^6 PFU per animal of $VSV_{\Delta GMT}$-$S_{\Delta 21}$ viruses in PBS or with PBS alone intranasally. At 0, 7, and 28 days postimmunization, mice were sacrificed with their spleens removed to perform ELISPOT assays.

All animal experiments were executed based on SHVRI (Shanghai Veterinary Research Institute) (SV-20211217-04) and SJTU (Shanghai JiaoTong University) ethical guidelines; All animals were identified as negative through serum neutralizing assay before study initiation.

2.14. Hematology, liver function, and renal function

The following indicators regarding animal hematology were examined in the study, including platelet (PLT), haemoglobin concentration (HGB), white blood cell-middle cell count (W-MCC), haematocrit neutrophil (HCT), white blood cell-large cell

Table 1 Animal experimental design of safety evaluation on hamster vaccinated by VSV_{MT}-Delta and VSV-Delta.

Animal	Inoculum	Route[a]	Immunization dose
LVG Golden Syrian Hamster	VSV_{MT}-Delta	IN	5×10^6 PFU
	VSV_{MT}-Delta	IN	5×10^5 PFU
	$VSV_{\Delta G}$-Delta	IN	5×10^6 PFU
	$VSV_{\Delta G}$-Delta	IN	5×10^5 PFU
	PBS	IN	/

[a]IN, intranasal inoculation. /, not applicable.

Table 2 Animal experimental design of immunology evaluation on hamster and hACE2-mouse vaccinated by $rVSV_{MT}$-$S_{\Delta 21}$.

Animal	Inoculum	Route	Immunization dose
LVG golden Syrian hamster	VSV_{MT}-WA1	IM[a]/IN[b]/*PO*[c]	10^5 PFU
	VSV_{MT}-Delta	IM/IN/*PO*	10^5 PFU
	VSV_{MT}-Omicron	IM/IN/*PO*	10^5 PFU
	VSV_{MT}-WA1	IM/IN/*PO*	10^6 PFU
	VSV_{MT}-Delta	IM/IN/*PO*	10^6 PFU
	VSV_{MT}-Omicron	IM/IN/*PO*	10^6 PFU
	PBS	IM/IN/*PO*	/
hACE2-mouse	VSV_{MT}-WA1	IM/IN/*PO*	10^6 PFU
	VSV_{MT}-Delta	IM/IN/*PO*	10^6 PFU
	VSV_{MT}-Omicron	IM/IN/*PO*	10^6 PFU
	PBS	IM/IN/*PO*	/

/, not applicable.
[a]IM, intramuscular injection.
[b]IN, intranasal inoculation.
[c]*PO*, Per os route inoculation.

count (W-LCC), the total white blood cell (WBC), mean corpuscular haemoglobin (MCH), mean corpuscular volume (MCV), mean corpuscular haemoglobin concentration (MCHC), red blood cells (RBC), white blood cell-small cell count (W-SCC), white blood cell-small cell ratio (W-SCR), red blood cell distribution width coefficient of variation (RDW-CV), white blood cell-middle cell ratio (W-MCR), white blood cell-large cell ratio (W-LCR) and red blood cell distribution width standard deviation (RDW-SD). The EDTA blood was collected and detected with the pocH-100iV Diff analyzer (Sysme).

Indicators associated with animal liver and renal function were also detected, including alkaline phosphatase (ALP), alanine aminotransferase (ALT), total-protein (TP, including albumin and globulin), gamma-glutamyl transferase (γ-GT), aspartate aminotransferase (AST), albumin (ALB), carbamide (UREA), uric acid (UA) and creatinine (CREA). The indicators were determined from serum with an automatic biochemical analyzer (Mindray BS360-S).

2.15. *Statistical analysis*

GraphPad Prism 8 and SPSS18 were used to analyze the data. An unpaired two-tailed *t*-test was used to compare the differences between the two groups. Two-way ANOVA statistical analyses among multiple groups were conducted. The value of $P < 0.05$ was credited with statistically significant.

Table 3 Animal experimental design of cellular immunity on hACE2 transgenic mice vaccinated by various $rVSV_{MT}$-$S_{\Delta 21}$ viruses.

Animal	Inoculum	Routes[a]	Immunization dose
hACE2 transgenic mice	VSV_{MT}-WA1	IN	10^6 PFU
	VSV_{MT}-WA1	IN	10^5 PFU
	VSV_{MT}-Delta	IN	10^6 PFU
	VSV_{MT}-Delta	IN	10^5 PFU
	VSV_{MT}-Omicron	IN	10^6 PFU
	VSV_{MT}-Omicron	IN	10^5 PFU
	VSV_{MT}-GFP	IN	10^6 PFU
	VSV_{MT}-GFP	IN	10^5 PFU
	PBS	IN	/

[a]IN, intranasal inoculation. /, not applicable.

3. Results

3.1. *Optimizing cytoplasmic tail of SARS-CoV-2 spike protein for construction of retargeting VSV_{MT} chimera virus*

SARS-CoV-2 S protein consists of the ectodomain, transmembrane and cytoplasmic tail (CT). It forms a homotrimer on the virion, and play a crucial role in mediating the virus's entry into human cells by binding to the cell-surface receptor angiotensin-converting enzyme 2 (ACE2). The CT domain of Spike protein is highly conserved among all the variants, whereas considerable mutations exist within the ectodomain among variants of concerns (VOCs) which leads to changes in protein conformation (Fig. 1A). Notably, there are ∼30 AA mutations occurring at the S protein ectodomain of Omicron variant (B.1.1.529) in comparison to that of classical WA1 strain, resulting in vaccine breakthrough.

The truncated tail of the coronavirus S protein can play a significant role in S protein incorporation efficiency into the VSV envelope membrane[27]. The CT domain of spike protein (S) of SARS-CoV-2 consists of 26 amino acids. Serial passaging of a cell-adapted $rVSV_{\Delta G}$-S demonstrated 19 or 21 amino acids truncation existed at the S protein cytoplasmic tail[28]. In our study, a strategy based on pseudotype entry assays of G-$rVSV_{\Delta G}$-GFP was set up to evaluate the efficiency of S with serially deleted cytoplasmic tail in rescuing retargeting VSV_{MT} chimera virus. With 19−26 amino acids of its carboxyl-terminal serially deleted (Fig. 1B), the mutant S genes of the SARS-CoV-2 WA1 strain were cloned into expression vector *p*IRES respectively. The resulting plasmids were designated as *p*IRES-$S_{\Delta 19}$, -$S_{\Delta 20}$, -$S_{\Delta 21}$, -$S_{\Delta 22}$, -$S_{\Delta 23}$, -$S_{\Delta 24}$, -$S_{\Delta 25}$, or -$S_{\Delta 26}$. Initially, the expression of these S mutants on the surface of transfected 293T cells was detected with flow cytometry assay and then normalized to a comparable level by adjusting the concentration of the transfected plasmid (Fig. 1C). A series of replication-defective pseudotype VSVs were generated through transduction with G-$VSV_{\Delta G}$-GFP at MOI of 1 as described[23], which were $S_{\Delta 19}$−$S_{\Delta 26}$-$VSV_{\Delta G}$-GFP, respectively.

The efficiency of the above S mutants packaging into the VSV envelope membrane was determined by counting the number of infected cells. Infective units (IU) of the VSV pseudotypes were determined and compared. As shown in Table 4, it was observed that the truncation of the S protein cytoplasmic tail could led to increased infectivity in comparison to full-length S (S_{FL}). The IU of VSV pseudotypes with $S_{\Delta 21}$ of WA1, Delta, and Omicron strains in hACE2-293T cells were 45.4 ± 5.72, 54.49 ± 10.22 or 48.42 ± 6.92, respectively. These were significantly higher than other S truncated mutants, such as $S_{\Delta 24}$ as well as the full-length S (S_{FL}). As a result, it suggested that with 21 amino acids at the carboxyl-terminal deleted, the mutant S protein ($S_{\Delta 21}$) can incorporate into VSV particles most efficiently.

To evaluate the intact antigenicity of the S mutant ($S_{\Delta 21}$) encoded by the VSV vector, recognition activities of $S_{\Delta 21}$ with hACE2 were characterized with specific neutralizing monoclonal antibodies. Among them, 2G1 was the one recognizing WA1 strain epitope, whereas the REGN10987 or 8G3 NAbs recognize epitopes of Delta or Omicron strains and potently inhibit their

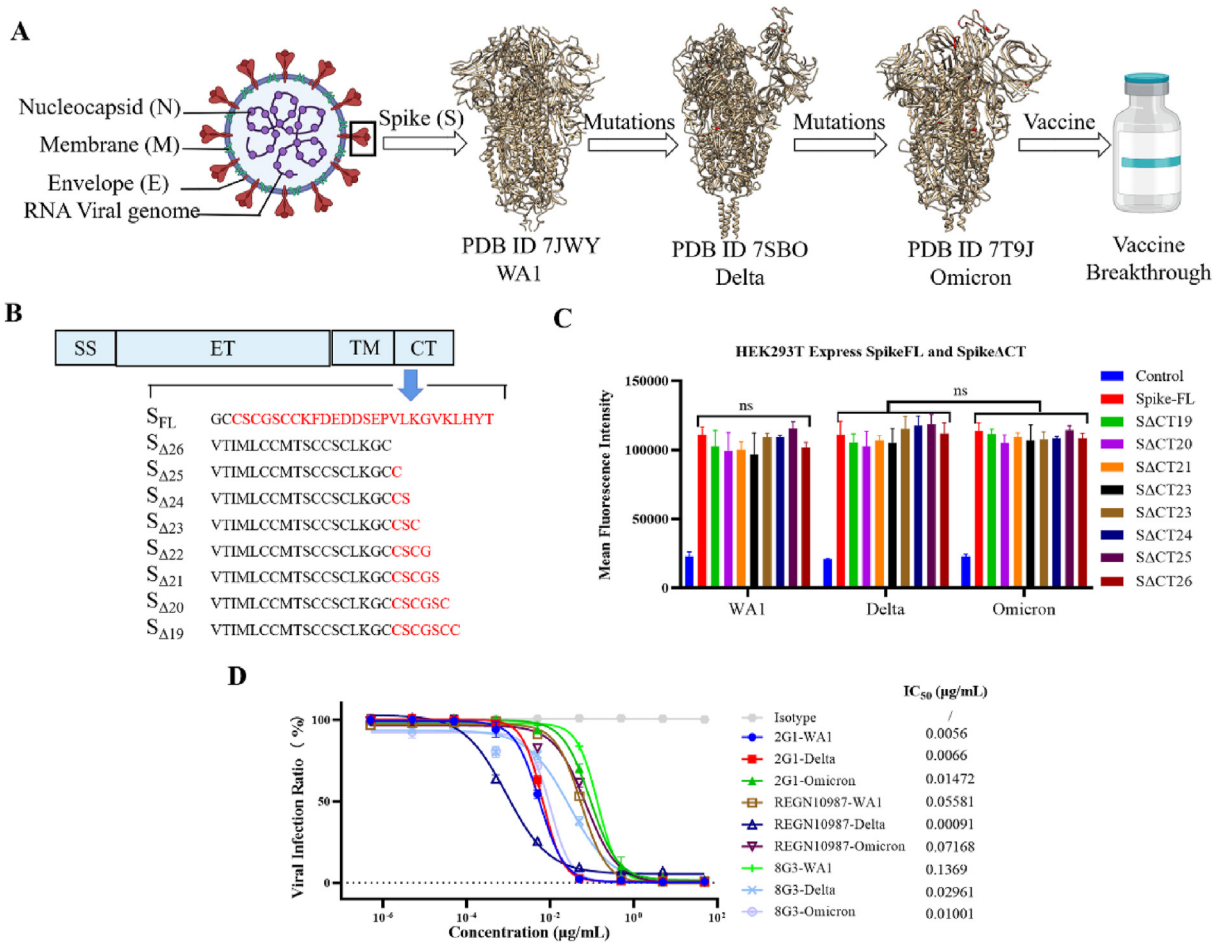

Figure 1 Characterization of the optimal cytoplasmic tail of SARS-CoV-2 spike protein for construction of retargeting VSV_{MT} chimera virus. Single-cycle VSV_S were pseudotyped with S mutants with different cytoplasmic tail lengths and were compared for their ability to mediate infection of ACE2-293T. (A) The spike protein conformations of WA1, Delta, and Omicron Variants. (B) SARS-CoV-2 S protein mutants with different cytoplasmic tail (CT) lengths. S_{FL}, $S_{\Delta26}$, $S_{\Delta25}$, $S_{\Delta24}$, $S_{\Delta23}$, $S_{\Delta22}$, $S_{\Delta21}$, $S_{\Delta20}$, and $S_{\Delta19}$ represent the full-length S protein or the S mutants with CTs truncated from 26 to 19 amino acids, respectively. The remaining CT regions are shown in red. SS, signal peptide sequence; ET, ectodomain; TM, transmembrane domain; CT, cytoplasmic tail. (C) Surface expression of S protein, S deletion mutants. At 24 h post-transfection, cells were subjected to a flow cytometry assay. (D) Intact antigenicity of the $S_{\Delta21}$ encoded by VSV vector. Binding activities of replication-defective $VSV_{\Delta G}$-GFP pseudotyped with $S_{\Delta21}$ were detected with neutralizing mAbs recognizing S protein, with the 2G1 against WA1 strain, REGN10987 or 8G3 recognizing Delta or Omicron variants, respectively. IC_{50} of the above mAbs against different VSV pseudotypes were calculated. Data are shown as mean ± SD with three replicates. ns means $P > 0.05$. Statistical significance was determined using two-way ANOVA with multiple comparisons.

infection respectively[29–31]. The IC_{50} of these antibodies was calculated using $S_{\Delta21}$-$rVSV_{\Delta G}$-GFP. Dilutions of the purified antibodies, 2G1, REGN10987, or 8G3, were pre-incubated with WA1, Delta, or Omicron $S_{\Delta21}$ protein pseudotyped VSV ($S_{\Delta21}$-$rVSV_{\Delta G}$-GFP) for 1 h at 37 °C and then infected hACE2-293T cells. As shown in Fig. 1D, the IC_{50} of 2G1 blocking of $S_{\Delta21}$-$rVSV_{\Delta G}$-GFP of WA1 was 0.0056 μg/mL, and those against Delta or Omicron $S_{\Delta21}$ pseudotyped viruses were 0.0066 μg/mL or 0.01472, respectively. The IC_{50} of REGN10987 blocking of $S_{\Delta21}$-$rVSV_{\Delta G}$-GFP of Delta was 0.00091 μg/mL, whereas it's blocking those of WA1 or Omicron were 0.05581 or 0.07168 μg/mL respectively. In addition, IC_{50} of 8G3 blocking of $S_{\Delta21}$-$rVSV_{\Delta G}$-GFP of Omicron was 0.01001 μg/mL, whereas the values of WA1 or Omicron were 0.13609 or 0.029061 μg/mL, respectively. Thus, it indicated that the truncation of 21 AA in the S protein intracellular domain has not affected its recognition activities by the corresponding neutralizing antibodies. Based on these findings, we hypothesized that the S mutant ($S_{\Delta21}$) expressed by the VSV vector retains its immunogenicity and could be dubbed as an authentic surrogate of SARS-CoV-2.

3.2. *Characterization of retargeting VSV_{MT} expressing truncated S protein of SARS-CoV-2 and its dominant VOCs*

There are two strategies to construct retargeting rVSV with its G protein replaced by foreign proteins, which are replication-competent or incompetent[23,32]. In contrast to the replication-incompetent pseudotyped virus, replication-competent rVSVs encoding SARS-CoV-2 S protein can propagate in the host, which consequently stimulates more potent immunities. Based on above study, 21 AA truncated S protein ($S_{\Delta21}$) has been identified as capable of incorporation into the VSV envelope efficiently not

Table 4 Infectivity units of non-replicating VSV ($\times 10^3$ IU/mL).

Truncated Spike proteins	WA1 -VSV$_{\Delta G}$-GFP	Delta -VSV$_{\Delta G}$-GFP	Omicron -VSV$_{\Delta G}$-GFP
Spike-FL	0.12 ± 0.09	0.12 ± 0.08	0.1 ± 0.06
SpikeΔCT19	29.42 ± 4.21	28.62 ± 6.51	25.62 ± 3.89
SpikeΔCT20	33.87 ± 5.34	30.90 ± 4.58	36.64 ± 3.50
SpikeΔCT21	45.4 ± 5.72	54.49 ± 10.22	48.42 ± 6.92
SpikeΔCT22	28.29 ± 4.58	42.06 ± 7.56	36.88 ± 5.31
SpikeΔCT23	34.47 ± 6.10	44.83 ± 7.65	31.37 ± 5.57
SpikeΔCT24	19.41 ± 3.46	25.26 ± 5.28	21.35 ± 4.51
SpikeΔCT25	11.16 ± 3.04	15.69 ± 4.80	10.75 ± 2.82
SpikeΔCT26	9.64 ± 3.46	8.29 ± 3.59	7.18 ± 2.37

Infectivity units were determined by counting GFP-expressing cells. Virus detections were repeated 5 times.

only for WA1 but also for the Delta and Omicron B1.1.529 variants. Thus, replication-competent rVSVs with its G replaced with $S_{\Delta 21}$ was rescued for the live vaccine candidates.

The recovery of rVSVs was performed as described in "Methods". Highly attenuated rVSVs, namely rVSV$_{\Delta GMT}$-WA1-$S_{\Delta 21}$-GFP (VSV$_{MT}$-WA1), rVSV$_{\Delta GMT}$-Delta-$S_{\Delta 21}$-GFP (VSV$_{MT}$-Delta) and rVSV$_{\Delta GMT}$-Omicron-$S_{\Delta 21}$-GFP (VSV$_{MT}$-Omicron), were successfully rescued (Fig. 2A). Individual plaques were isolated and the potentially retargeting rVSVs were propagated and characterized with Western blotting. Cell lysates were collected and identified with both S protein-specific antibodies as well as VSV convalescent sera from infected mice. With S protein-specific antibody, the expected-sized band of ~200 kD was detected in VSV$_{MT}$-WA1, VSV$_{MT}$-Delta and VSV$_{MT}$-Omicron infected VeroE6 cells (Fig. 2B), whereas the corresponding band was not detected in wild-type VSV (VSV-GFP) infected cells. With VSV-infected mouse convalescent sera as the primary antibody, VSV structural G protein was not identified in the retargeting rVSVs infected VeroE6 cells, whereas N/P protein was detected. In the VSV-GFP control group, the VSV structural protein G and the N/P were all detected (Fig. 2C). These results indicated that the G protein was successfully replaced by $S_{\Delta 21}$ in the retargeted rVSVs.

Because ACE2 is the receptor of SARS-CoV-2, the tropism of rescued chimeric viruses (VSV$_{MT}$-WA1, VSV$_{MT}$-Delta, and VSV$_{MT}$-Omicron) was initially determined with cells stably expressing hACE2 or not. In the study, hACE2-BHK21 were infected with the above rVSV$_{\Delta GMT}$-$S_{\Delta 21}$ chimera viruses or wild-type viruses (VSV-GFP) at MOI of 1, with BHK21 cells as the control. GFP-positive cells, indicating infection by VSV$_{MT}$-WA1, VSV$_{MT}$-Delta, and VSV$_{MT}$-Omicron, were observed in hACE2-BHK21 cells, rather than in BHK21 cells (Fig. 2D). In addition, GFP-positive cells can be detected in both hACE2-BHK21 and BHK21 cells infected with VSV-GFP. The infectivity of rVSV-SARS-CoV-2 chimera viruses was further tested on different cell lines. In SARS-CoV-2 permissive human Huh7 cells along with hACE2-BHK21 cells, high infectivity was observed (Fig. 2E), whereas in non-permissive Hela, HT-29 cells or A549 cells, no apparent infection signal was detected compared with mock control ($P < 0.01$) (Fig. 2E). The result indicated that retargeting VSV$_{MT}$ with $S_{\Delta CT21}$ allows specific infection of host cells through hACE2 receptor. Syncytium formations were also compared among the rVSVs. With ten syncytia selected randomly, the mean areas mediated by various S proteins were observed. As shown in Fig. 2F and I, syncytia formed by VSV$_{MT}$-Delta were ~2-fold larger than those formed by VSV$_{MT}$-WA1, and 5-fold larger than those formed by VSV$_{MT}$-Omicron in hACE2-293T cells. A similar tendency has been observed in VeroE6 cells, although the syncytia formed by three rVSVs were smaller in contrast to those in hACE2 cells. The result was consistent with those shown by Zhao et al.[33], which indicated that the Omicron variant shows less fusogenic in comparison with the Delta variant in TMPRSS2 positive cells.

Replication efficiency of $S_{\Delta 21}$-based retargeting VSV$_{MT}$ was characterized by one-step growth curves in VeroE6 cells, which were infected with VSV$_{MT}$-WA1, VSV$_{MT}$-Delta, or VSV$_{MT}$-Omicron at a MOI of 3. Triplicate supernatants which sampled at the indicated time points were titrated by plaque assays. The titers of all rVSVs increased after inoculation, with VSV$_{MT}$-Delta exhibiting the highest replication efficiency compared with VSV$_{MT}$-WA1 and VSV$_{MT}$-Omicron. As shown in Fig. 2G, VSV$_{MT}$-Delta reached its highest titers as early as 12 h.p.i., which is around 3.6×10^6 PFU/mL, whereas VSV$_{MT}$-WA1 can reach its peak titer of around 2.2×10^6 PFU/mL at about 24 h post-infection. Of note, VSV$_{MT}$-Omicron can reach the highest titers at about 24 h.p.i., which was around 8.3×10^5 PFU/mL. The maximum differences in replication titers for the viruses occurred at 8 h.p.i. to 12 h.p.i. As shown by Fig. 2G, at 8 h.p.i., the titers of VSV$_{MT}$-Omicron could be 7×10^2 PFU/mL, whereas the titers of VSV$_{MT}$-Delta and VSV$_{MT}$-WA1 was 5.6×10^5 PFU/mL and ~2×10^5 PFU/mL, respectively. At 12 h.p.i., the title of VSV$_{MT}$-Delta was 2.5×10^6 PFU/mL, the title of VSV$_{MT}$-WA1 was ~2.5×10^5 PFU/mL, and the titer of VSV$_{MT}$-Omicron was ~4.4×10^4 PFU/mL. Thus, of the rVSVs tested, the retargeting rVSVencoding S protein of the Delta variant indicated the highest replication efficiency, whereas the VSV$_{MT}$-Omicron showed the lowest. Comparable results were also observed in plaque assay. Areas of plaques (means ± SD) generated by the different rVSV$_{\Delta GMT}$-$S_{\Delta 21}$ viruses were calculated. VSV$_{MT}$-Delta forms much bigger plaques (average size of ~3.83 mm^2) than VSV$_{MT}$-WA1 (average size of 0.42 mm^2) and VSV$_{MT}$-Omicron did (average size of ~0.10 mm^2) (Fig. 2H). As a result, the replication efficiency of the rVSVs *in vitro* followed the tendency of VSV$_{MT}$-Delta > VSV$_{MT}$-WA1>VSV$_{MT}$-Omicron.

3.3. *Quality assessment of virions after ultra-centrifugation*

High-quality virions are essential for our vaccine study. Thus, a method for rapid and morphology-preserving purification of rVSV$_{\Delta GMT}$-$S_{\Delta 21}$ virions with sucrose gradient ultracentrifugation was used[34]. As shown in Fig. 3A, clearly concentrated corresponding viral proteins were displayed in the purified rVSV$_{\Delta GMT}$-$S_{\Delta 21}$ virions while the unpurified supernatant samples showed a diffuse background. In purified rVSV$_{\Delta GMT}$-$S_{\Delta 21}$ virions, the G protein (~68 kD) of VSV was not detected, whereas clear spike proteins of SARS-CoV2 (~200 kD) did (Fig. 3A). In contrast, in purified VSV-GFP virions, the G protein rather than the spike protein could be discerned. In addition, bands (~50 kD) corresponding to VSV nucleocapsid protein (N) and matrix protein (~27 kD) were discerned in both the rVSV$_{\Delta GMT}$-$S_{\Delta 21}$ and VSV-GFP virion. Thus, the results indicated that the rVSV$_{\Delta GMT}$-$S_{\Delta 21}$ virions can be purified with sucrose gradient ultracentrifugation.

Previous studies reported that ultracentrifugation could lead to some adverse effects on viral morphology and structural integrity, such as influenza virus[35]. In our study, the intact structure of the ultracentrifugation concentrated rVSV$_{\Delta GMT}$-$S_{\Delta 21}$ virions were identified by electron microscopy. Importantly, despite the

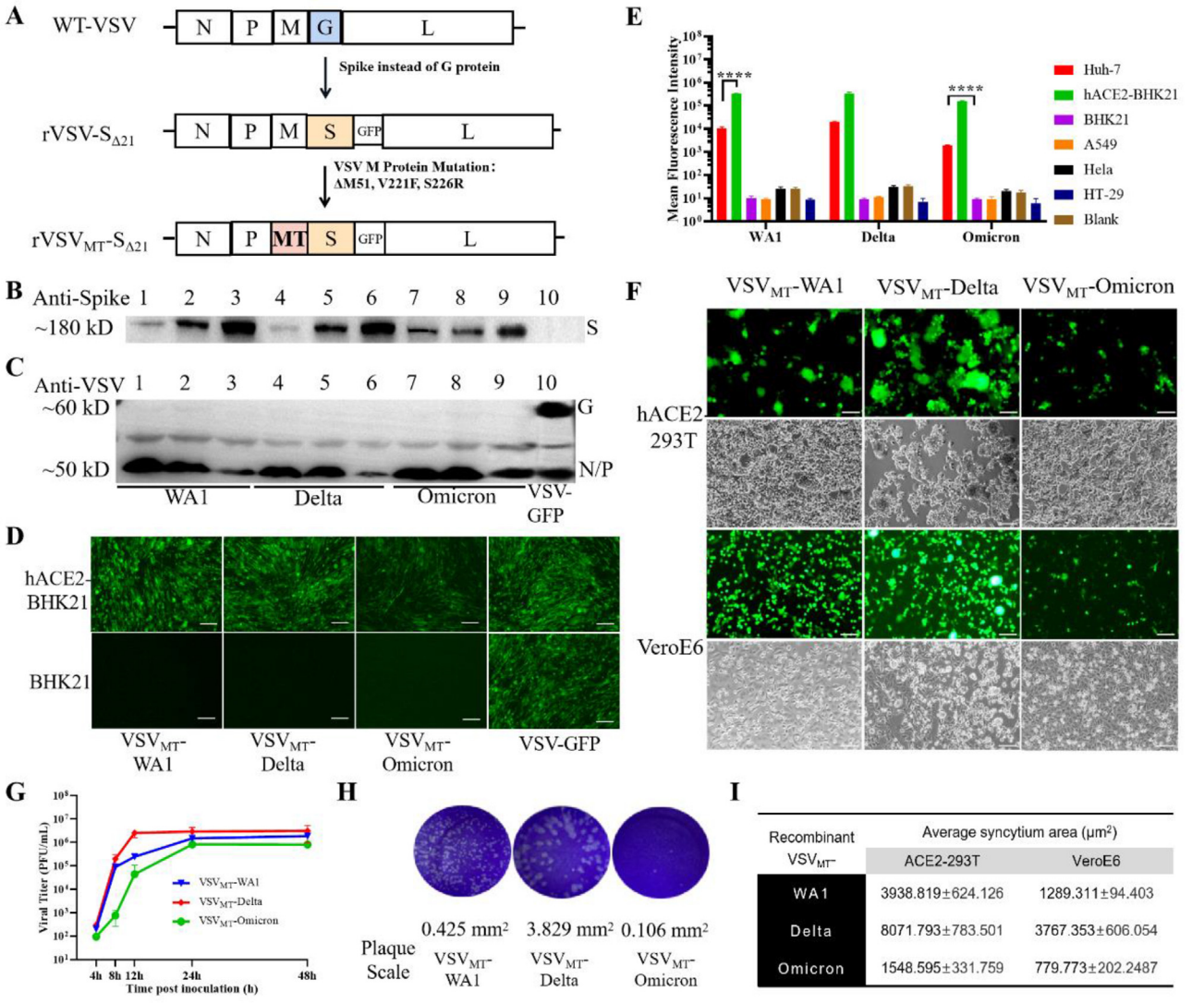

Recombinant VSV$_{MT}$-	Average syncytium area (μm²)	
	ACE2-293T	VeroE6
WA1	3938.819±624.126	1289.311±94.403
Delta	8071.793±783.501	3767.353±606.054
Omicron	1548.595±331.759	779.773±202.2487

Figure 2 Generation of retargeting VSV$_{MT}$ encoding S protein of various strains. (A) Diagram of retargeting VSV$_{MT}$ construct. Wild-type VSV has no S gene insertion; rVSV$_{MT}$-S$_{\Delta 21}$ encodes for SARS-CoV-2 S mutants of various strains with their genome. The parental VSV$_{MT}$ genome encodes the nucleoprotein (N), phosphoprotein (P), glycoprotein (G), RNA polymerase (L), and mutant M protein (MT) that harbors three mutations (ΔM51, V221F, and S226R). The gene for the truncated S protein of WA1, variants of Delta or Omicron (S$_{\Delta CT21}$) were used to replace the G gene of the VSV through Mlu I and XhoI enzyme digestion, eGFP gene was cloned into the sites with XhoI and NheI enzyme digestion. (B, C) Western blotting of rescued rVSV$_{MT}$-S$_{\Delta 21}$ chimera viruses. (B) S protein was detected using a specific antibody; (C) with VSV convalescent sera. The viruses were passaged in VeroE6 cells. Lanes 1, 2, and 3 represented collected cells infected with VSV$_{MT}$-WA1 of passages 1, 5, and 10, respectively; Lanes 4, 5, and 6 represented those infected with VSV$_{MT}$-Delta of passages 1, 5, 10; lines 7, 8, 9 represented those infected with VSV$_{MT}$-Omicron of passages 1, 5, 10; line 10 represented VSV-GFP control. (D) Selective infection of hACE2-positive cell lines. hACE2-BHK21 and BHK21 cells were infected with rVSV$_{MT}$-S$_{\Delta 21}$ chimera viruses or VSV$_{MT}$-GFP at MOI of 1. Twenty-four hours post-infection, GFP expression of infected cells was photographed by a fluorescence microscope. (E) Infectivity of different cell lines with rVSV$_{MT}$-S$_{\Delta 21}$ chimera viruses. Mean Fluorescent Intensity (MFI) was calculated. (F) Syncytia formation of rVSV$_{MT}$-S$_{\Delta 21}$ chimera viruses in different host cells. Virus-induced cytopathic effects are shown in the photomicrographs above. Confluent hACE-293T and VeroE6 cell monolayers were infected with VSV$_{MT}$-WA1, VSV$_{MT}$-Delta, and VSV$_{MT}$-Omicron at an MOI of 1. Photographs were taken 24 h after infection. Syncytia mediated by the viruses were shown. (G) One step growth curve of rVSV$_{MT}$-S$_{\Delta 21}$ chimera viruses. VeroE6 cells were infected with VSV$_{MT}$-WA1, VSV$_{MT}$-Delta, and VSV$_{MT}$-Omicron at MOI of 3. Plaque titrations from the indicated time points were performed with VeroE6 cells. (H) Plaque size formed by recombinant VSVs in VeroE6 cells. Plaques in Vero cells infected with VSVs. Ten individual plaques were selected randomly to calculate the areas. Images were acquired 24 h post-infection (h.p.i). (I) The average syncytium area (μm^2) was evaluated by Image J. ****$P < 0.0001$. Statistical significance was determined using two-way ANOVA with multiple comparisons. Above data are shown as means ± SD ($n = 3$).

replacement of their original G proteins with S proteins, the virions can keep the bullet-shape morphology and maintain their morphological integrity (Fig. 3B).

The rVSV$_{\Delta GMT}$-S$_{\Delta 21}$ vaccine candidates were constructed based on replication-competent VSV$_{MT}$, which had been attenuated due to the triple mutations occurring at amino acid position

ΔM51, V221F, and S226R of matrix protein in comparison to wild-type VSV. In the study, VSV_{MT}-WA1, VSV_{MT}-Delta, and VSV_{MT}-Omicron seed viruses were amplified in the production cell VeroE6 with their M genes sequenced. As described by de Haan et al.[24], with a classical method based on viral stock passaging, enough amounts of random plaque identification, the genetic stability of the $rVSV_{\Delta GMT}$-$S_{\Delta 21}$ matrix protein gene was confirmed. As shown in Fig. 3C, with wild type VSV M gene as the control, all plaques randomly selected from passages 5 and 10 of each viral stock exhibited consistent modified bases modified bases at amino acid position ΔM51, V221F, and S226R in $rVSV_{\Delta GMT}$-$S_{\Delta 21}$ viruses. No back mutations in the M protein gene were observed after serial passaging.

In summary, based on assessments including SDS-PAGE, electron microscopy observation, as well as matrix gene stability analysis, it indicated that high-quality $rVSV_{\Delta GMT}$-$S_{\Delta 21}$ virions have been successfully prepared, making them suitable for subsequent animal vaccine study.

3.4. $rVSV_{MT}$ indicated improved safeness in contrast to wild-type VSV as the vector encoding SARS-CoV-2 spike protein

VSV has been proved as a promising vaccine and oncolytic vector; however, high-dosed wild-type VSV can cause neurological deficits in animals, especially *via* the intranasal route[36]. Thus, potential pathogenicity resulting from infection of VSV_{MT} and wild-type VSV encoding Spike protein of Delta variant was initially evaluated in hamsters, which inoculated intranasally at a dose as high as 5×10^6 PFU/100 μL. The reason to select the Delta variant lies in that it indicates higher virulence than the other known VOC strains[37]. Of note, our study also confirmed that $rVSV_{MT}$ encoding Delta strain Spike protein possessed the highest replication efficiency and syncytial formation among the strains tested *in vitro*. The dose of 5×10^6 PFU/100 μL depended on its maximum dose that could be prepared by us for $rVSV_{MT}$-Delta in a 100 μL volume.

Hamsters were inoculated with $rVSV_{MT}$-Delta or rVSV-Delta intranasally at doses of 5×10^5 or 5×10^6 PFU/100 μL. Daily monitoring of body-weight changes was performed for 28 days, and the organs, including the testis and spleen, were checked. In addition, liver and kidney function-associated indicators were also evaluated. No treatment-related mortality was observed in administrated animals. As shown in Fig. 4A, the body-weight of hamsters treated with $rVSV_{MT}$-Delta steadily increased post-infection, similar to the PBS group. In contrast, rVSV-Delta-treated animals lost weight significantly at both doses of 5×10^5 PFU and 5×10^6 PFU. Notably, at 5 days post inoculation (d.p.i), the body weight loss caused by rVSV-Delta could arrive at 8% in the 5×10^6 PFU group.

According to a previous report, SARS-CoV-2 infection has been associated with testicular damage in humans[38]. Furthermore, the mean length and thickness of the spleen decrease in some patients who emerged from SARS-CoV-2. Thus, potential damage to the testis and spleen due to rVSV-Delta or $rVSV_{MT}$-Delta infection was checked in the study. At 28 d.p.i., the weights of testis were ~1.7 g in hamsters treated with $rVSV_{MT}$-Delta at a dose of 5×10^6 PFU, comparable to that in the PBS group. In contrast, the weights of testis reduced to around 1.5 g in animals

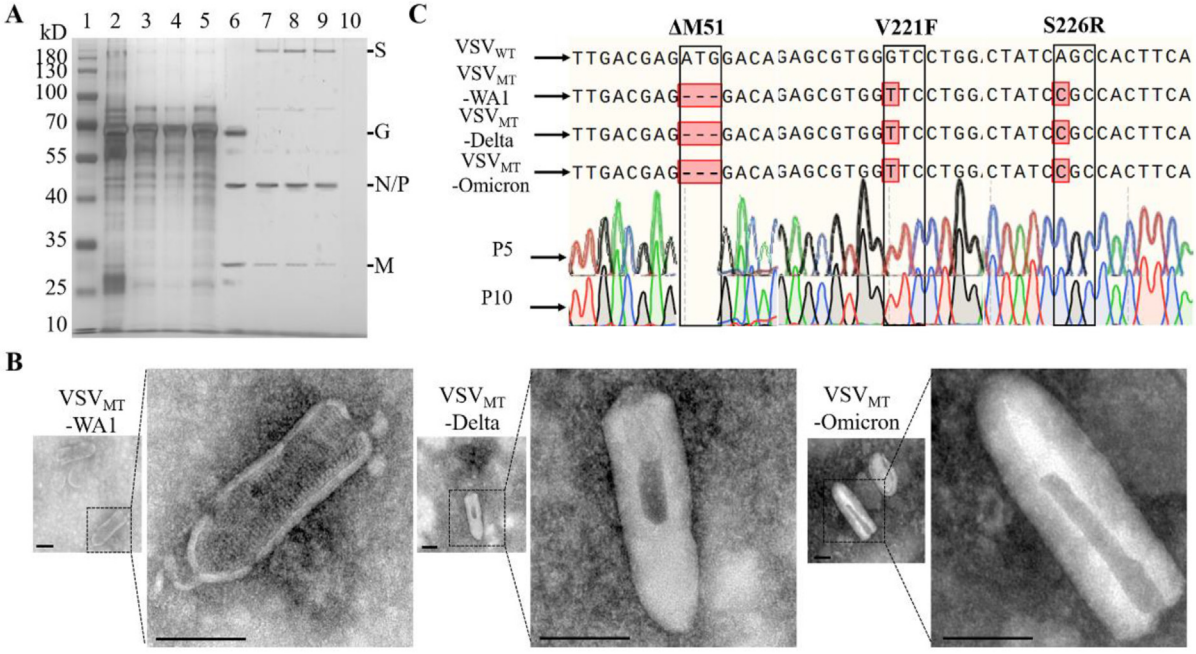

Figure 3 Purification of $rVSV_{\Delta GMT}$-$S_{\Delta 21}$. VeroE6 Cells were infected $rVSV_{\Delta GMT}$-$S_{\Delta 21}$. The supernatants were concentrated by sucrose gradient ultracentrifugation. through a 20% (*w*/*w*) sucrose cushion at 90,000 × *g* for 1.5 h at 4 °C. The pelleted virions were then suspended in DPBS. (A) Concentrated $rVSV_{MT}$-$S_{\Delta 21}$ were separated by SDS-PAGE and visualized by silver nitrate staining. Lane 1 is the protein marker; lanes 2, 3, 4, 5 represent collected cells infected with VSV-GFP, VSV_{MT}-WA1, VSV_{MT}-Delta, VSV_{MT}-Omicron respectively; lanes 6, 7, 8, 9 represent purified virions of VSV-GFP, VSV_{MT}-WA1, VSV_{MT}-Delta, VSV_{MT}-Omicron respectively; line 10 represents control group. (B) Negatively stained representative electron micrographs of VSV_{MT}-WA1, VSV_{MT}-Delta, and VSV_{MT}-Omicron virions. (C) M gene sequence analysis of $rVSV_{\Delta GMT}$-$S_{\Delta 21}$ viruses from plaques purified from the serial passage of 5 or 10.

treated with rVSV-Delta at a dose of 5×10^6 PFU ($P < 0.05$) (Fig. 4B). With regards to the spleen, the weights were around 0.15 g in all groups, with no difference observed at 28 d.p.i. (Fig. 4C and D). The effects of $rVSV_{MT}$-Delta, as well as rVSV-Delta on liver and kidney function, were also examined at 28 d.p.i.. With the concentration of alanine aminotransferase (ALT), albumin (ALB), carbamide (UREA), and creatinine (CREA) in sera as the indicators, no significant difference was identified between the groups treated with $rVSV_{MT}$-Delta, rVSV-Delta and PBS control (Fig. 4E−H and Supporting Information Fig. S1). A series of blood routine tests demonstrated that $rVSV_{MT}$-Delta and rVSV-Delta did not lead to obvious changes in the examined indicators (Supporting Information Fig. S2). However, some testicular damage was observed in high-dosed rVSV-Delta- treated hamsters.

In summary, the results indicated that $rVSV_{MT}$ demonstrated improved safety in contrast to wild-type VSV as the vector encoding SARS-CoV-2 spike protein.

3.5. *Immunogenicity of chimeric $rVSV_{\Delta GMT}$-$S_{\Delta 21}$ viruses in hamsters via mucosal routes*

ACE2 is moderately expressed in the respiratory tract and highly in the intestinal tract of humans. Both tissues can be the invasion sites for SARS-CoV-2. Thus, we focused on the significance of mucosal routes in inducing SARS-CoV-2 specific immune

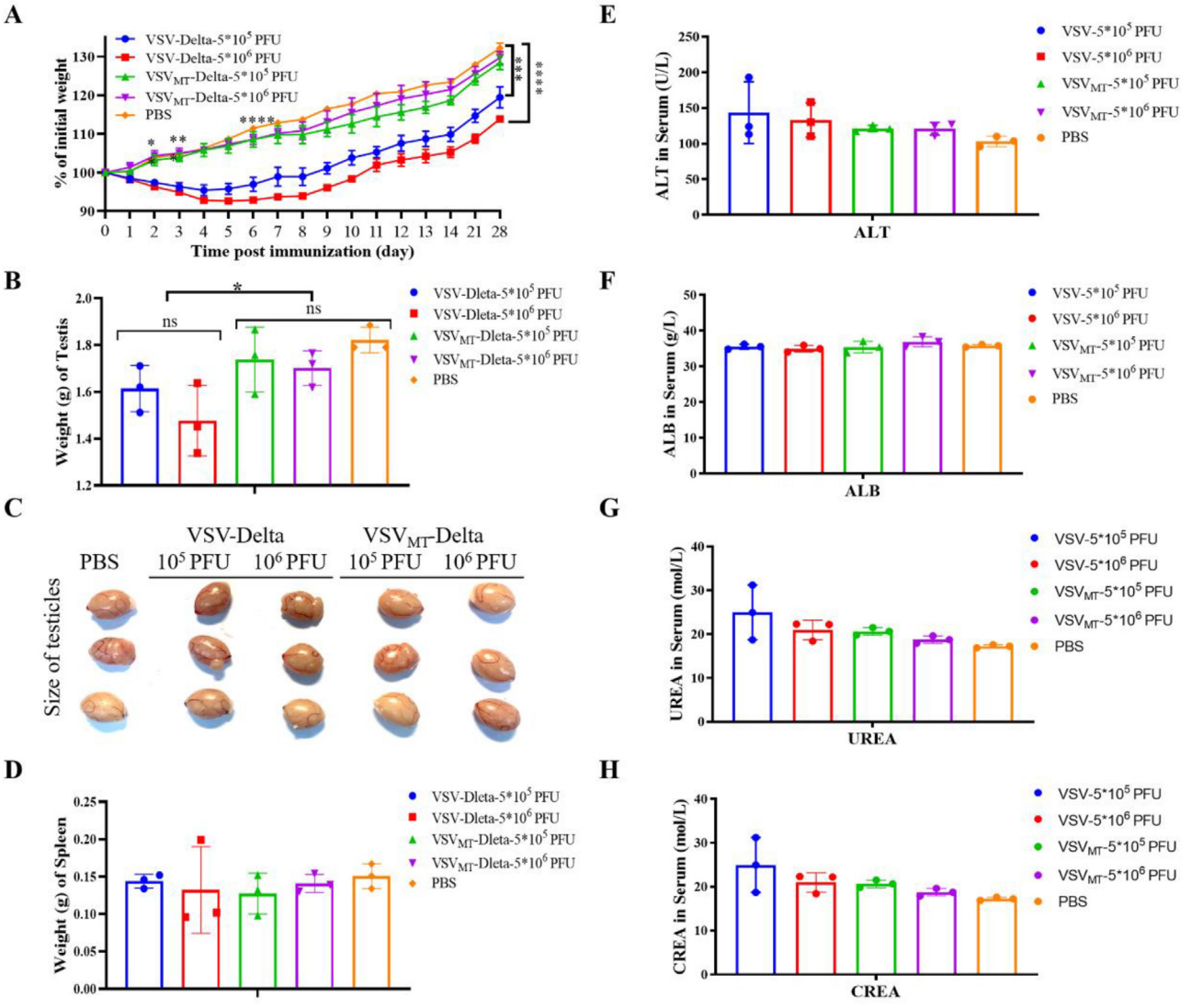

Figure 4 Safety evaluation of VSV_{MT} in contrast to wild-type VSV as the vectors encoding spike protein. Healthy hamsters were inoculated with VSV-Delta or VSV_{MT}-Delta at doses of 5×10^5, and 5×10^6 PFU/hamster *via* intranasal routes, with PBS buffer as the control. Body weight loss was monitored daily until 28 days. On 28 d.p.i., animal sera and organs including testis and spleen were also collected. (A) Body weight change of inoculated hamsters. (B) Weight of testis collected from animals on 28 d.p.i. (C) Testis collected from animals at 28 d.p.i. (D) Indicators regarding liver and kidney functions in animal sera collected at 28 d.p.i. Alanine aminotransferase (ALT), albumin (ALB), carbamide (UREA), and creatinine (CREA) were determined with an automatic biochemical analyzer (E−H). ns, $P > 0.05$; $^*P < 0.05$, $^{***}P < 0.001$, $^{****}P < 0.0001$. Data are shown as mean ± SD ($n = 3$). Statistical significance was determined using two-way ANOVA with multiple comparisons.

responses by various rVSV$_{\Delta GMT}$-S$_{\Delta 21}$ viruses. Antibody responses stimulated by the live rVSV$_{\Delta GMT}$-S$_{\Delta 21}$ viruses were evaluated in the collected samples of serum and bronchoalveolar lavage fluid. Golden syrian hamsters were administrated with rVSV$_{\Delta GMT}$-S$_{\Delta 21}$ (VSV$_{MT}$-WA1, VSV$_{MT}$-Delta, or VSV$_{MT}$-Omicron) *via* mucosal routes of intranasal or *per oral* (*PO*) at doses of 1×10^5 or 1×10^6 PFU/hamster, with the intramuscular route as the control. Three animals were used in each group, and their body weight changes were monitored daily. In addition, morbidity including ruffled fur, lethargy, and hunched posture were also monitored. Blood specimens were gathered from animals on 0, 7, and 28 days post-immunization (d.p.i). Immunized animals were euthanized at 28 d.p.i., with bronchoalveolar lavage fluid (BALF) and tissues harvested for evaluation. Neutralization antibodies against various strains of SARS-CoV-2 in serum and BALF samples were also detected with the above corresponding rVSV$_{MT}$-S$_{\Delta 21}$ viruses that expressed GFP protein. Titers were negative before study initiation as well as in the mock-infected hamsters.

Serum antibody responses in animals administrated rVSV$_{\Delta GMT}$-S$_{\Delta 21}$ viruses indicated a dose-dependent manner (Fig. 5 and Table 5). In each group of animals, the NAb titers at a dose of 1×10^6 PFU are higher than those at 1×10^5PFU ($P < 0.01$). However, after vaccination with the same dose, neutralizing Ab (NAb) titers were rapidly induced at 7 d.p.i, but did not increase significantly at 28 d.p.i in most of the groups (Fig. 5 and Table 5). This indicated that the antibodies could be stimulated by VSV$_{MT}$-encoded S protein early point post-inoculation, similar to those shown in the rVSV-based Ebola vaccine. Of note, the administration route of the rVSVs could play an important role in stimulating NAb *in vivo*. Much higher NAb titers in sera could be induced *via* IN than IM or *PO* routes. For example, in the animals immunized intranasally with VSV$_{MT}$-Delta at a dose of 1×10^6 PFU, the NAb titers were 5254.0 ± 212.7 at 7 d.p.i., and 13,995.0 ± 6088.21 at 28 d.p.i., respectively. When animals were administrated with the same dose of VSV$_{MT}$-Delta *via* IM route, the NAb titers were 1379.9 ± 657 at 7 d.p.i., and 1701.6 ± 188.4 at 28 d.p.i., respectively, roughly 10-fold lower than IN route. Similar trends were also observed in other rVSVs (Fig. 5 and Table 5). In contrast, although antibodies could be elicited in animals by all three rVSV$_{\Delta GMT}$-S$_{\Delta 21}$ viruses *via* the oral route, whereas much lower than IN and IM routes. The highest titers of neutralizing antibodies in sera induced by *PO* routes were observed in VSV$_{MT}$-WA1, which was 594.5 ± 947.0 at 7 d.p.i., and 386.9 ± 584.0 at 28 d.p.i., when at a dose of 1×10^6 PFU. However, the large SD values suggested that the mechanism still needs to be identified, although the *PO* route may be potentially promising for delivering VSV-based COVID-19 vaccine, due to the high ACE2 expression in small intestine tissues.

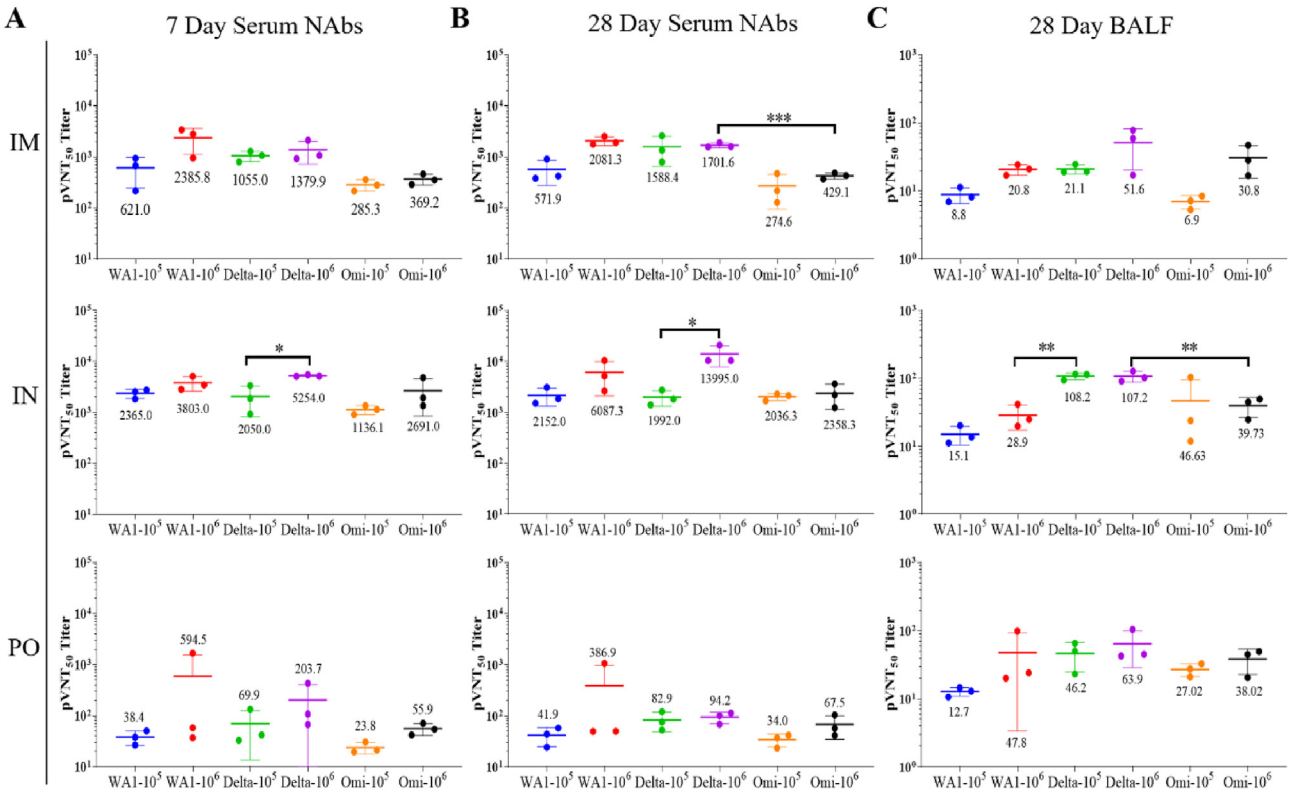

Figure 5 Antibody responses in serum and bronchoalveolar lavage fluid (BALF) samples after immunization. The immunogenicity of VSV$_{MT}$-WA1, VSV$_{MT}$-Delta, or VSV$_{MT}$-Omicron was determined in the hamsters immunized at a single dose of 10^5 PFU or 10^6 PFU *via* IN, IM, or *PO* routes. PBS was used as the mock control. Sera were collected on 0, 7, and 28 days post inoculation (d.p.i). BALF were harvested on 28 days post-inoculation. Serum and BALF neutralization titers were quantified using VSV$_{MT}$-WA1, VSV$_{MT}$-Delta, or VSV$_{MT}$-Omicron respectively. The titers were expressed as the reciprocal of the highest dilution of antibody giving a 100% inhibition of cytopathic effect. The plots show the geometric mean with geometric standard deviation ($n = 3$). (A, B) NT values of sera samples from hamsters vaccinated *via* different routes. Samples were collected on 7 d.p.i (a); and 28 d.p.i (b). (C) NT values of BALF samples from hamsters vaccinated *via* different routes. Samples were collected on 28 d.p.i.. *$P < 0.05$, **$P < 0.01$, ***$P < 0.001$. Statistical significance was determined using two-way ANOVA with multiple comparisons.

Table 5 Hamster serum and BALF neutralizing antibody titers.

Recombinant VSVs	route	7-day post vaccination			28-day post vaccination					
		Serum			Serum			BALF		
		10^5 PFU	10^6 PFU	Mock	10^5 PFU	10^6 PFU	Mock	10^5 PFU	10^6 PFU	Mock
VSV_{MT}-WA1	IM	612.0 ± 366.3	2385.8 ± 1269.4	<5	571.9 ± 294.1	2081.3 ± 404.7	<5	8.8 ± 2.3	20.8 ± 3.7	<2
	IN	2365.0 ± 476.7	3803.0 ± 1183.5	–	2152.0 ± 831.0	6087.3 ± 3976.0	–	15.1 ± 4.7	28.9 ± 11.4	–
	PO	38.4 ± 12.0	594.5 ± 947.0	–	41.9 ± 16.9	386.9 ± 584.0	–	12.7 ± 1.9	47.8 ± 44.5	–
VSV_{MT}-Delta	IM	1055.0 ± 242.7	1379.9 ± 657.2	–	1588.4 ± 930.7	1701.6 ± 188.4	–	21.1 ± 3.2	51.6 ± 31.3	–
	IN	2050.0 ± 1226.2	5254.0 ± 212.7	<5	1992.0 ± 681.7	13995.0 ± 6088.2	<5	108.2 ± 12.0	107.2 ± 19.0	<2
	PO	69.9 ± 56.3	203.7 ± 201.7	–	82.9 ± 34.4	94.2 ± 23.4	–	46.2 ± 21.3	63.9 ± 35.0	–
VSV_{MT}-Omicron	IM	285.3 ± 72.0	369.2 ± 86.6	–	274.6 ± 179.6	429.1 ± 59.0	–	6.9 ± 1.6	30.8 ± 15.4	–
	IN	1136.1 ± 222.4	2691.0 ± 1842.3	–	2036.3 ± 314.6	2358.3 ± 1200.8	–	46.6 ± 50.0	39.7 ± 13.1	–
	PO	23.8 ± 6.1	55.9 ± 14.5	<5	34.0 ± 9.6	67.5 ± 33.0	<5	27.0 ± 5.9	38.3 ± 15.6	<2

–not applicable.

Among the attenuated rVSV encoding various S proteins, it indicated that VSV_{MT}-Delta can induce the most potent antibody responses. Omicron is the one with more potent transmissibility than other known strains[39]. However, the antibody responses induced by VSV_{MT}-Omicron were significantly lower than those induced by VSV_{MT}-Delta and VSV_{MT}-WA1. The detailed mechanism also needs further study, although our *in vitro* results demonstrated that the replication efficiency as well as the syncytium formation by VSV_{MT}-Omicron indicated a significant reduction in contrast to the other two rVSVs.

The levels of neutralization antibody (NAb) in BALF are often used as an important indicator for evaluating the effect of mucosal immune responses. Circulating S-specific B and T cell immunity could be induced by mRNA-based vaccine. However, in COVID-19 convalescents, these immune responses were attenuated in BALF of vaccinated individuals[40]. In BALF, despite the generally lower NAb levels observed compared to those in sera, the levels of IN route were still higher than those of IM routes, consistent with the results observed in sera samples, especially in VSV_{MT}-Delta administrated animals. As shown, the neutralizing antibodies in BALF induced by VSV_{MT}-Delta through IN route were 108.2 ± 12.0 in the 10^5 PFU group and 107.2 ± 19.0 in the 10^6 PFU group, whereas in IM groups, the Ab titers were 21.1 ± 3.2 in the 10^5 PFU group and 51.6 ± 31.3 in the 10^6 PFU group. As a result, our studies support the mucosal immunity achieved *via* intranasal delivery. Strikingly, although the levels were very low, the *PO* route demonstrated its efficacy in eliciting mucosal antibodies, as shown in BALF samples collected from the three $rVSV_{\Delta GMT}$-$S_{\Delta 21}$ viruses (Fig. 5 and Table 5).

3.6. No significant adverse effect was observed in hamsters administrated with the VSV_{MT}-based COVID-19 vaccine candidates

Hamsters were administrated *via* intranasal, intramuscular, or *PO* at increasing doses of $rVSV_{MT}$ encoding $S_{\Delta 21}$ protein of WA1, Delta, or Omicron strain. The doses used were 1×10^5, or 1×10^6 PFU/hamster, with PBS as the control. Adverse effects in animals were examined, which included body weight changes, liver and kidney function. In particular, histopathology and the potential presence of the $rVSV_{\Delta GMT}$-$S_{\Delta 21}$ viruses in the lung were detected. Accordingly, gross pathological changes in tissues/organs or other abnormalities were observed and recorded.

Body weight changes and morbidity were monitored daily until 28 d.p.i.. Following administration, neither treatment-related mortality nor noticeable local or systemic reactions were observed in animals inoculated with the $rVSV_{\Delta GMT}$-$S_{\Delta 21}$ viruses. As shown in Fig. 6A–C, the administrated animals exhibited a mean group body weight gain and showed no signs of morbidity, similar to that of the control group, suggesting that the tested viral doses were safe. SARS-CoV-2 infection develops typically as a respiratory disease in humans[41], leading to severe interstitial pneumonia along with alveolar septa thickening and massive infiltration of inflammatory cells. Liver and kidney damage are also identified as typical occurrences in COVID-19 patients[42–44]. Because $rVSV_{\Delta GMT}$-$S_{\Delta 21}$ viruses have been probed to use hACE2 as the cellular entry receptor, potential adverse effects due to the replication-competent rVSVs infection were examined in the organs of the lung, liver, and kidney. Macroscopic examinations indicated that at 28 d.p.i., no treatment-related adverse macroscopical changes in the above organs were observed (not shown). In particular, similar to mock control, histopathological evaluation of lung tissues indicated that

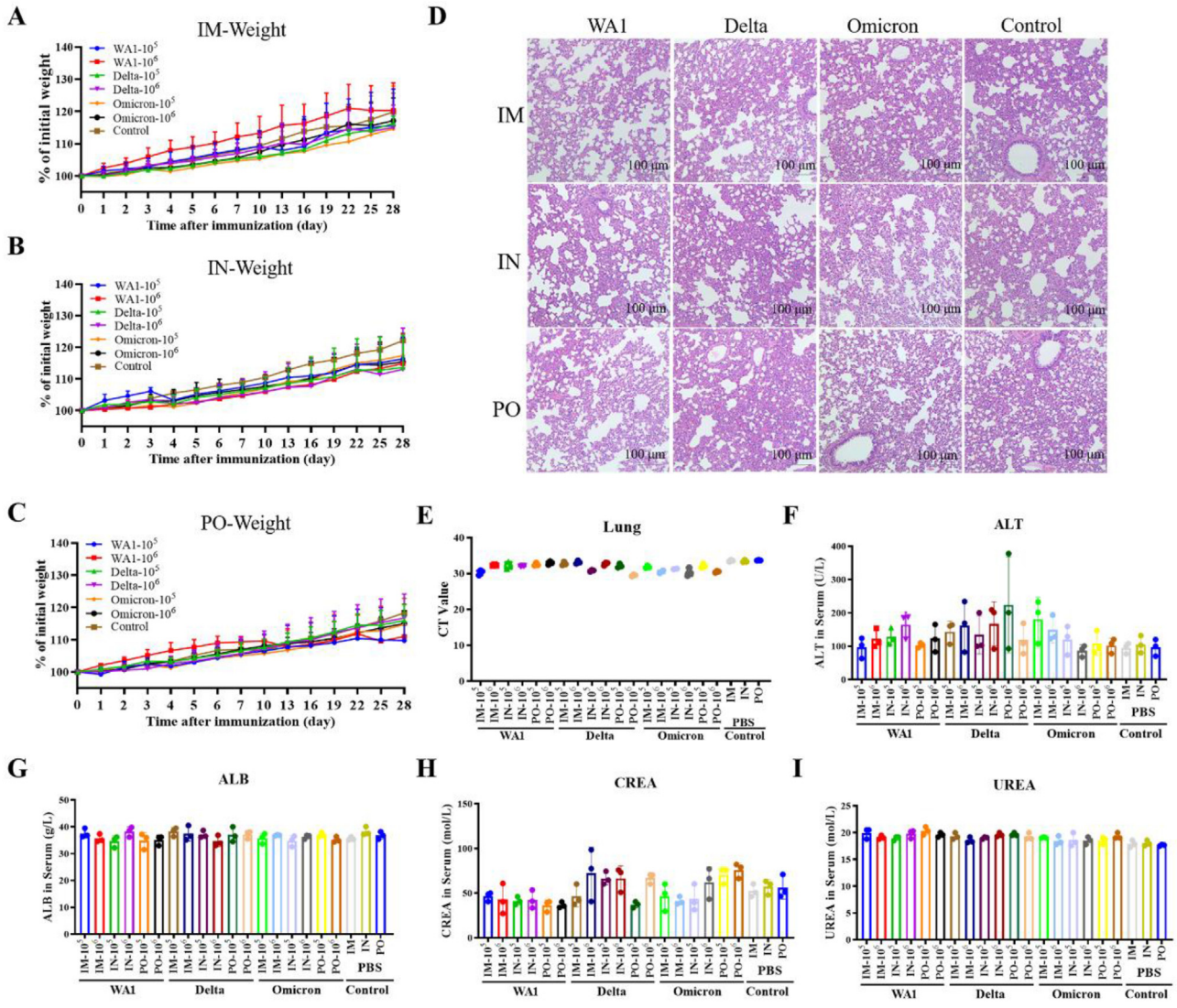

Figure 6 Safety evaluation of chimeric rVSVs encoding the spike of WA1, Delta, and Omicron strain on administrated hamsters. Healthy hamsters were inoculated with VSV_{MT}-WA1, VSV_{MT}-Delta, or VSV_{MT}-Omicron at doses of 10^5,10^6 PFU/hamster *via* IN, *PO*, or IM routes, with PBS buffer as the control. Body weight loss was monitored daily until 28 days. Lung tissues were collected on 28 d.p.i. and examined. Data are shown as means ± SD ($n = 3$). (A−C) Body weight changes of vaccinated hamsters. (D) Representative hematoxylin and eosin (H&E) staining of lung sections from hamsters collected from administrated groups at a dose of 10^6 PFU at 28 d.p.i.. (E) The VSV N gene CT value was determined by RT-qPCR with lung tissues collected at 28 d.p.i.. (F−I) Evaluation of liver and kidney function in hamsters. Alanine aminotransferase (ALT), albumin (ALB), carbamide (UREA), and creatinine (CREA) were determined with an automatic biochemical analyzer. ns, $P > 0.05$; $^*P < 0.05$, $^{****}P < 0.0001$. Statistical significance was determined using two-way ANOVA with multiple comparisons.

the alveolar structure was intact. No hemorrhage was observed in animal blood vessels, and no inflammatory cell infiltration was identified in the lungs from all the $rVSV_{\Delta GMT}$-$S_{\Delta 21}$ treated animals (Fig. 6D). With VSV N gene as the marker by RT-qPCR, the CT values in the lung of the vaccinated animals were also determined. As it was shown, no significant difference was found among all groups ($P > 0.05$) (Fig. 6E). In addition, symptoms such as vomiting and diarrhea were not observed after vaccination.

The effects of the $rVSV_{\Delta GMT}$-$S_{\Delta 21}$ Viruses infection on liver and kidney function were examined with sera collected at 28 d.p.i, according to the baseline of the indicators. With regards to liver functions, alkaline phosphatase (ALP), serum alanine aminotransferase (ALT), total-protein (TP, including albumin and globulin), aspartate aminotransferase (AST), albumin (ALB) and gamma-glutamyl transferase (γ-GT) were detected. As shown, among the indicators detected, no significant difference was observed ($P > 0.05$) between the $rVSV_{\Delta GMT}$-$S_{\Delta 21}$ vaccinated groups and the control group (Fig. 6F and G and Supporting Information Fig. S3). In addition, the indicators regarding kidney functions of creatinine (CREA) and carbamide (UREA) also demonstrated no significant changes compared to the control group (Fig. 6H, I and Fig. S3). Thus, the $rVSV_{\Delta GMT}$-$S_{\Delta 21}$ viruses indicated no adverse effect against the potentially targeted organs such as lung *via* all the tested routes.

In clinical, some SARS-CoV-2 vaccines can lead to rare- and vaccine-associated thrombosis and thrombocytopenia, which has been called vaccine-induced thrombotic thrombocytopenia

(VITT)[45,46]. Herein, a series of blood routine tests show that the rVSV$_{\Delta GMT}$-S$_{\Delta 21}$ vaccines did not lead to significant changes in blood indicators regardless of the administrated route (Supporting Information Fig. S4).

In summary, according to the clinical, histopathologic, and hematological data, it demonstrated that is safe at the tested doses regardless of the immune routes.

3.7. Cross-reactivity of NAbs in immunized hamsters induced by chimeric rVSV encoding S proteins of various SARS-CoV-2 strains

Vaccine design against emergent VOCs in pan-coronaviruses is the main aim for the next-generation COVID-19 vaccine. The existence of broadly neutralizing antibodies (bNAbs) to coronaviruses (CoVs) suggests the possibility of making a broad-spectrum vaccine. It was reported by Tang et al.[47] recently that sequential immunization with mucosal adenovirus-S vaccination boosted strong cross-neutralizing antibody responses after systemic mRNA vaccination, not only for the ancestral virus but also for the Omicron variant, which may be due to the heterologous prime and boost procedure. As a promising vaccine vector, it is currently unclear the extent of cross-neutralizing antibody responses induced by VSV$_{MT}$-WA1, VSV$_{MT}$-Delta, or VSV$_{MT}$-Omicron, respectively.

The cross-reactivity of serum NAb titers between VSV$_{MT}$-WA1, VSV$_{MT}$-Delta, or VSV$_{MT}$-Omicron was tested. Sera with high neutralizing antibody levels collected on 7 and 28 d.p.i were selected and used to measure their cross-protection against heterologous strains. As shown in Fig. 7, in VSV$_{MT}$-WA1 IN samples, the homologous NAb mean titers were 2723. In contrast, the mean titers of cross-neutralization titers against VSV$_{MT}$-Delta or VSV$_{MT}$-Omicron were 225 or 101, respectively, which were 12-fold or 27-fold reduced (Fig. 7A). The results could be due to more mutations accumulated in Spike protein of Omicron variant in compared to that of Delta strain. A similar tendency has been observed in other samples. In sera from VSV$_{MT}$-Delta administrated animals, the cross-neutralization titers against VSV$_{MT}$-WA1 or VSV$_{MT}$-Omicron were reduced by 20-fold or 22.24-fold, respectively (Fig. 7B). In sera from animals administered with VSV$_{MT}$-Omicron, the cross-neutralization titers of the samples against VSV$_{MT}$-WA1 or VSV$_{MT}$-Delta were 14-fold and 16-fold reduced, respectively (Fig. 7C). As a results, neutralization activity was significantly reduced in all samples when reacting with heterologous S protein-based rVSVs. The existing vaccines, which are mainly made with S of classical WA1 strain, may not provide enough protection against the emerging variants. In addition, the cross-neutralizing antibody protection between Delta and Omicron is also very low, suggesting the two strains might have originated differently. It has been reported that the Omicron strain may have originated from immune-deficient patients. The result indicates the complexity of future COVID-19 epidemics. Therefore, in terms of occurrence time, the Omicron emerged and circulated not far from the Delta strain, but the cross-protection of neutralizing antibodies between them was also poor. The S protein

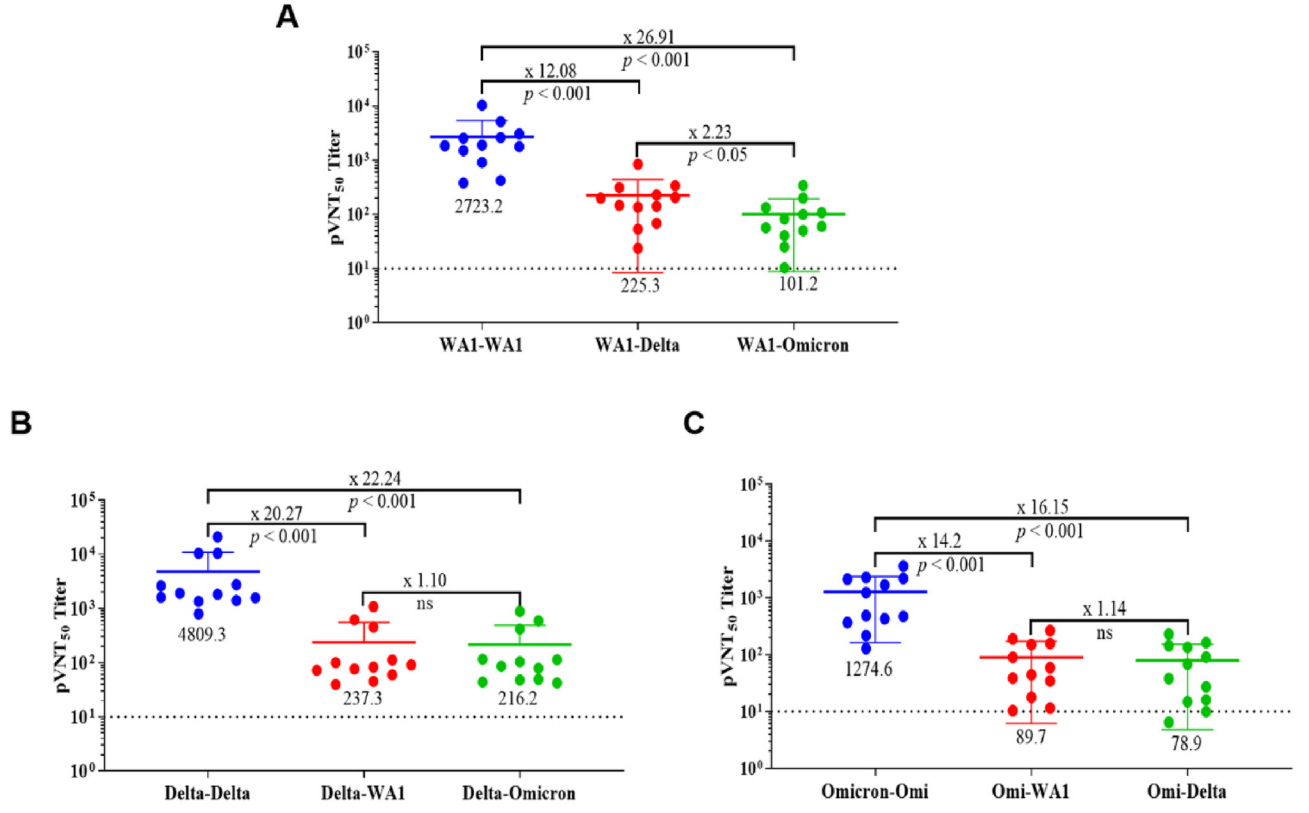

Figure 7 Cross-reactivity among sera antibodies collected from animals vaccinated with VSV$_{MT}$ encoding various S proteins of various SARS-CoV-2 strains. Sera were collected from VSV$_{MT}$-WA1 (A), VSV$_{MT}$-Delta (B) or VSV$_{MT}$-Omicron (C) administrated animals as above. Their neutralization titers against VSV$_{MT}$-WA1, VSV$_{MT}$-Delta, or VSV$_{MT}$-Omicron were determined. The titers were expressed as the reciprocal of the highest dilution of antibody giving a 100% inhibition of cytopathic effect. The plots show the geometric mean with geometric standard deviation ($n = 12$).

from Delta strain dose not seems suitable for developing vaccines for the Omicron variant.

3.8. *The rVSV$_{MT}$-based COVID-19 vaccine candidates can stimulate comprehensive immune responses effectively in hACE2 transgenic mice*

The human ACE2 transgenic mouse is another commonly used animal model for evaluating COVID-19 vaccines. In our study, the transgenic mouse model was set up with hACE2 expression controlled by the mouse ACE2 promoter (Supporting Information Fig. S5A). High levels of hACE2 expressions were detected in the intestine and kidney tissue, while it was moderately expressed in the lung and upper respiratory tract tissue (Fig. S5B and S5C). The expression characteristics are similar with those of humans (Fig. S5D). Consistent with the protocol used in hamsters, as shown above, the hACE2 transgenic mice were inoculated with the rVSV$_{\Delta GMT}$-S$_{\Delta 21}$ viruses at a single dose of 1×10^6 PFU/mouse through intranasal (IN), *PO*, or intramuscular (IM) routes. Animal body weights were monitored daily for two weeks. Sera, as well as BAL fluid, were collected at 28 d.p.i., with neutralization antibody titers (NAb) detected. As shown in Fig. 8A, the administrated animals exhibited body weight gain with all viruses tested *via* IN, *PO*, or IM routes.

As shown in Fig. 8B, neutralization antibody levels stimulated by the chimeric rVSV$_{\Delta GMT}$-S$_{\Delta 21}$ viruses in hACE2 transgenic mice demonstrated dependence on the S protein source as well as administration route. In sera collected at 28 h.p.i., neutralization activity could be elicited by the rVSV$_{\Delta GMT}$-S$_{\Delta 21}$ candidates *via* IN, IM, and *PO* routes. However, with the same virus, serum antibody titers induced in the IM and *PO* groups were lower than those induced *via* the IN route. For example, in VSV$_{MT}$-Delta vaccinated transgenic mice, the NAb titer induced *via* IN route was 689.2 ± 206.1, whereas in sera *via PO* or IM routes, the titers were 279.0 ± 91.6 or 395.0 ± 142.1, respectively. Of note, in BALF samples, VSV$_{MT}$-Delta can induce significantly higher NAb titers *via* the IN and *PO* routes than IM route, which were 120.5 ± 27.9, 114.6 ± 34.2 or 43.6 ± 10.8, respectively. The same tendency was also observed in the other rVSVs, which was consistent with the results identified in hamsters. Because neutralizing antibody levels in BALF samples usually reflect mucosal immune responses, it is reasonable to assume that the IN and *PO* administration routes are effective in eliciting mucosal immunity in transgenic mice. Among the chimeric rVSV$_{MT}$ encoding various S proteins, differences in their immunogenicity were also observed (Fig. 8B). The NAb titer levels followed the tendency of VSV$_{MT}$-Delta > VSV$_{MT}$-WA1> VSV$_{MT}$-Omicron in sera as well as BALF samples.

Cell-mediated immune responses generated by rVSV$_{\Delta GMT}$-S$_{\Delta 21}$ *via* the intranasal route in hACE2 transgenic mice were further measured with IFN-γ ELISPOT, which was also dependence on the S protein source and dose. As shown in Fig. 8C and D, the rVSV$_{\Delta GMT}$-S$_{\Delta 21}$ can stimulate statistically significant ($P < 0.01$) cellular immune responses against SARS-CoV2 S1 and S2 peptide pool as compared with VSV-GFP and PBS controls. Among all the viruses tested, higher T-cell responses could be stimulated in VSV$_{MT}$-Delta-immunized mice than in other two strains ($P < 0.01$). In contrast, no significant differences were observed in animals immunized with VSV$_{MT}$-Omicron and VSV$_{MT}$-WA1 immunized at the same dose at 7 or 28 d.p.i.. In the animals vaccinated with the same virus, the T-cell responses were significantly higher in the 10^6 PFU group than in the 10^5 PFU group ($P < 0.01$). Interestingly, a higher level of IFN-γ expression in the splenic T lymphocytes was detected by the ELISPOT assay when stimulated *in vitro* with the S1 peptide pool as opposed to the S2 pool, which might be due to the presence of immunodominant T cell epitope in S1 domain. The representative spot of the ELISPOT assay was also shown in supporting Information Fig. S6 and Table S2.

In summary, consistent with the above results in hamsters, the rVSV$_{MT}$-based COVID-19 vaccine candidates can effectively stimulate comprehensive SARS-CoV-2 specific immune responses in hACE2 transgenic mice.

4. Discussion

As a promising mucosal vaccine candidate for countering COVID-19, the safety of replicative rVSV vector is of concern. To overcome this obstacle, we replaced the G protein gene in the VSV genome with a mutant S protein gene (S$_{\Delta 21}$) from various SARS-CoV-2 strains and introduced three mutations in the M protein of VSV, including S226R, V221F, and ΔM51 (VSV$_{MT}$). The VSV$_{MT}$ has shown sufficient safety in previous studies, demonstrating its significantly hampered capacity to inhibit the type I interferon (IFN) signaling pathway and suppress host gene expression compared to wild-type VSV[22]. Thus, our study takes advantage of VSV$_{MT}$ as a safe vaccine vector aiming at activating mucosal immunity to counter the threat of SARS-CoV-2.

To date, there have been at least two clinical trials involving the preparation of COVID-19 vaccines based on VSV vectors, motivated by VSV$_{\Delta G}$-ZEBOV-GP efficacy. However, V590, which was developed by Merck company, demonstrated low immunogenicity with single intramuscular administration in seronegative participants[48]. This result might be due to that ACE2 is expressed at a low level in muscle tissue cells. So, we focused on mucosal delivery of rVSV$_{MT}$ expressing S proteins *via* nasal and *PO* routes, taking advantage of the ideal expression of ACE2 in the tissues. Furthermore, all known vaccines based on VSV vectors nowadays are developed with spike protein of the parental WA1 strain. VOCs such as Delta and Omicron are of extreme concern because of their virulence and transmissibility. In the study, the immunogenicity of the rVSV chimeric virus, encoding S$_{\Delta 21}$ of Omicron, Delta as well as WA1 strain, was investigated and compared in various animal models, which have not been reported before. Additionally, different outcomes due to the conformational changes within various spike proteins, such as fusion activity, were also characterized with the help of the replicative chimeric VSVs.

The Delta variant is regarded as the most virulent among the VOCs, whereas the Omicron variant, a novel SARS-CoV-2 lineage B.1.1.529, is the most transmissible[49], which might be related to the conformational changes of spike proteins[50]. The S protein of the Omicron variant accumulates >30 mutations compared to the parental WA1 strain, many of which can be associated with its transmissibility and immune escape[49,51]. SARS-CoV2 spike protein directs viral attachment by binding cellular receptor ACE2. Afterward, cellular TMPRSS2, or proteases such as Cathepsins B and L in the endosome mediate cleavage of the Spike to activate fusion between the viral and cellular membranes, which allows the virus core to entry the cell cytoplasm. Our *in vitro* study showed that cell fusion ability directed by S proteins of WA1 and VOC strains differed significantly. As shown by the study, the replication and syncytium formation followed the tendency of VSV$_{MT}$-Delta > VSV$_{MT}$-WA1>VSV$_{MT}$-Omicron. VSV$_{MT}$-Delta possessed potent replication and fusogenic ability in host cells. The result is consistent

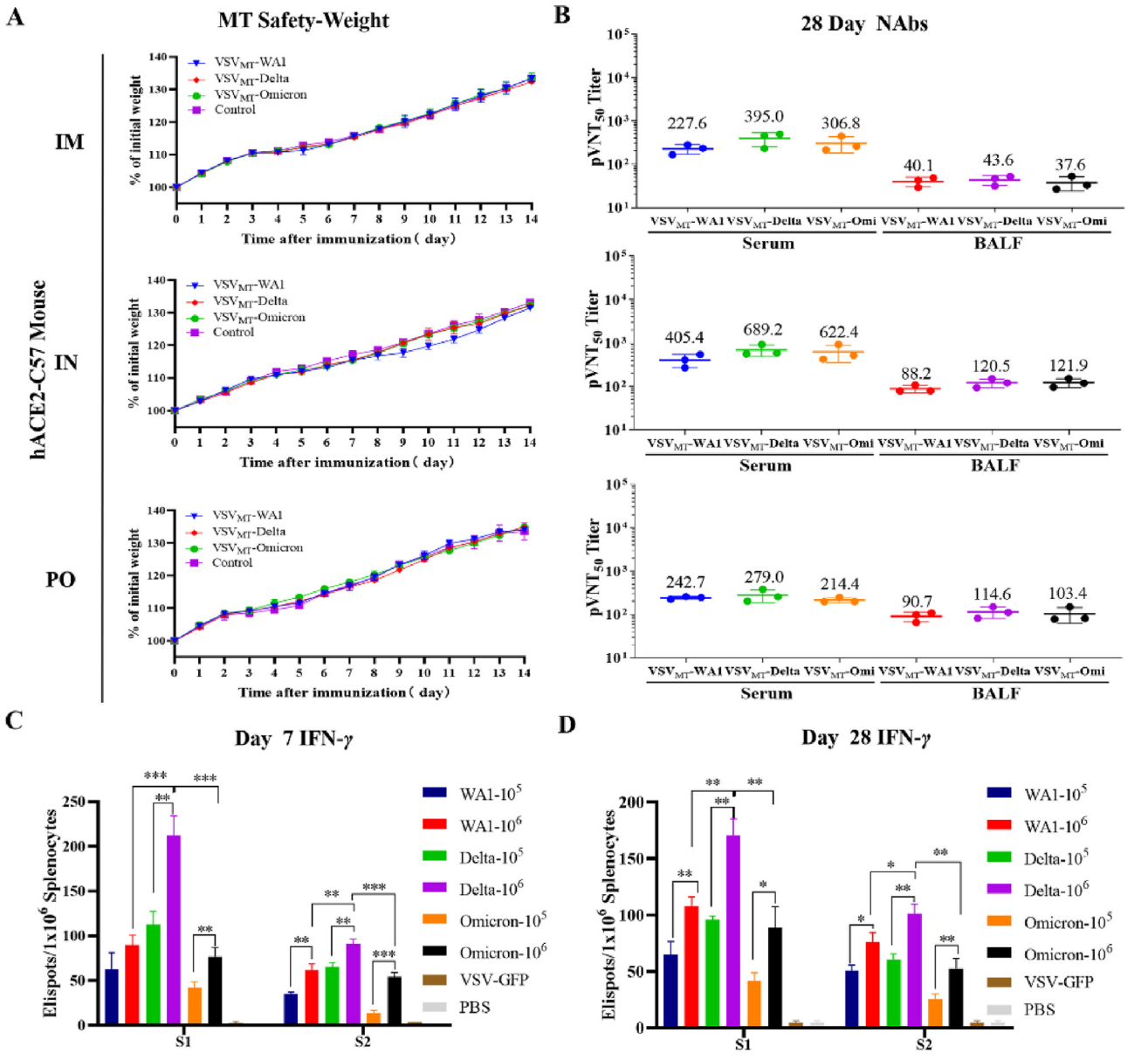

Figure 8 Immunogenicity of VSV$_{MT}$-WA1, VSV$_{MT}$-Delta, and VSV$_{MT}$-Omicron in hACE2-Mouse by vaccination route. hACE2-Mouse were intranasally (IN), intramuscularly (IM) or orally (*per oral*, *PO*) vaccinated with a single dose of VSV$_{MT}$-Delta, VSV$_{MT}$-WA1, or VSV$_{MT}$-Omicron at 1×10^6 PFU/50 μL. (A) The body weight changes of the immunized mice were monitored daily until 14 d.p.i.. (B) Serum and BALF neutralizing antibody titers collected on 28 d.p.i.. The titers were expressed as the reciprocal of the highest dilution of antibody giving a 100% inhibition of cytopathic effect. The plots show the geometric mean with geometric standard deviation. (C, D) S-specific cellular-mediated immune responses. Splenectomies were performed on mice sacrificed at 7 d.p.i (C); and 28 d.p.i (D), following responses with rVSV$_{\Delta GMT}$-S$_{\Delta 21}$ *via* intranasal route vaccination. VSV-GFP as well as PBS controls were also included. The results are presented as mean ELISPOTS per million splenocytes any background ELISPOTS from unpulsed mock controls standard deviation from the means. $^*P < 0.05$. $^{**}P < 0.01$. $^{***}P < 0.001$. Data are shown as means ± SD ($n = 3$). Statistical significance was determined using two-way ANOVA with multiple comparisons.

with the reports that the Omicron strain shows much less fusogenic compared with Delta, which might be due to the difference in entry pathway between Omicron and Delta variants[52]. Omicron variant infection is mainly mediated *via* the endocytic pathway rather than enhanced by TMPRSS2[33]. Because syncytia formation itself is an important way for viruses to escape host immunity, this also may have an impressive implication for the Delta variant on the manifestations or disease severity in clinical[53]. The detailed protein motif, as well as the amino acid sites associated with the mechanism, deserve further investigation.

In our study, the spike protein expression obtained from the VSV$_{MT}$-S variants was sufficient to generate high NAb titers in hamster models *via* routes of IN, *PO*, and IM. Unlike the results reported in humans by Robbins et al.[48], our experiments showed that a single shot of rVSV$_{\Delta GMT}$-S$_{\Delta 21}$ *via* the intramuscular route can induce considerable neutralization activity in hamsters *via* the IM route using all the three chimeric rVSVs, including the classical WA1 strain. Of note, we also revealed the superior immunogenicity of a single IN dose of VSV$_{\Delta GMT}$-S$_{\Delta 21}$ compared to a single IM or *PO* dose of VSV$_{MT}$-Variants. IN vaccination with all

the $VSV_{\Delta GMT}$-$S_{\Delta 21}$ viruses resulted in serum and BALF neutralization antibody titers exceeding those in animals vaccinated by IM injection. Furthermore, we demonstrated the generation of cell-mediated immune responses by $rVSV_{\Delta GMT}$-$S_{\Delta 21}$ *via* intranasal administration in animals. Thus, as the important indicator for mucosal immune responses, the presence of high-titer neutralizing antibodies in BALF samples as shown by our studies reveals the key role of intranasal immunization with VSV_{MT}-based COVID-19 vaccines. The results might be attributed to the spike-dependent chimeric VSV infection and replication in the respiratory tract mucosa. Consistent with our findings, it has also been shown that compared to COVID-19 convalescents, healthy individuals inoculated with mRNA vaccines had significantly lower levels of neutralizing antibodies in the BALF, despite robust S-specific antibody responses in the blood[47]. Strikingly, serum neutralization antibody titers were also detected in BALF samples in animals administrated *via PO* routes, although lower compared to than IN route. The result could be attributed to the high levels of hACE2 expression in the intestine, suggesting the possibility of developing a COVID-19 vaccine *via* the oral route. Optimal carriers for the gastrointestinal delivery of the rVSV vaccine may serve as an alternative solution to improve efficacy.

Previous clinical reports suggest that SARS-CoV induces stronger humoral immune responses than SARS-CoV-2[54,55]. We also demonstrated that the immunogenicity of the $rVSV_{\Delta GMT}$-$S_{\Delta 21}$ vaccine candidates was strain-dependent. Our *in vivo* study in both hamster and transgenic mice models indicated that the immunogenicity of VSV_{MT}-Omicron was significantly lower than that of VSV_{MT}-Delta and VSV_{MT}-WA1. The immunogenicity of VSV_{MT}-Delta ranks the highest, which indicates not only humoral immunity and mucosal immunity but also cellular immunity. This result is consistent with the different replication efficiency of the $rVSV_{MT}$-$S_{\Delta 21}$ viruses *in vitro*, potentially resulting from the conformational changes among S proteins of various COVID-19 strains.

Facing the challenge of rapid mutation of SARS-CoV-2, some challenges remain to be resolved in future studies, such as the development of a universal vaccine. At present, vaccines are mostly based on the classical WA1 strain. However, our results demonstrated that the cross-reactivity reduced significantly among various $rVSV_{MT}$-$S_{\Delta 21}$ viruses, especially between VSV_{MT}-WA1 versus VSV_{MT}-Omicron. The genetic distance between the Omicron strain and the classical strain was significant. This result suggested that the existing vaccines based on the classical strain are not sufficient to protect against Omicron variant infection due to the genetic distance between Omicron and WA1 train. Although the occurrence time of the Omicron and Delta variants was less than one year, the cross-neutralization activity induce by their S protein is also very low. Thus, it seems that the Delta variant is not suitable for developing a vaccine against the Omicron strain. Sequential vaccinations which combine the VSV_{MT}-based Omicron vaccine candidate with the currently licensed inactivated vaccine or mRNA vaccine might be a promising strategy to improve the efficacy of VSV_{MT}-based Omicron vaccine candidate, as well as provide cross-protection among various variants of concern.

5. Conclusions

In summary, we successfully generated a series of mucosal vaccine candidates to counter COVID-19 based on a highly attenuated VSV_{MT} vector. In animal models of hamster and hACE2-mouse, it was demonstrated that a single-dose intranasal immunization with the vaccines can elicit effective mucosal and cellular immunity with full rein safety. Considering the urgent need to develop mucosal vaccines against SARS-CoV2 infection, in particular the Omicron strain as well as its emerging variants, $rVSV_{MT}$ can be the promising platform for commercial mucosal vaccines.

Acknowledgments

This work was supported by Biomedicine and Technology Supporting Project of Shanghai Science and Technology Innovation Plan (Grant Nos. 22S11902200 and 20S11904900, China) and Open grant of Engineering Research Center of Cell & Therapeutic Antibody, Ministry of Education, Shanghai Jiao Tong University (Grant No. 19X110020009-003, China).

Author contributions

Conception and design: Tao sun, Baohong Zhang, Yong Ke and En Zhang. Yong K, En Zhang, Jianming Guo, Xiaoxiao Zhang, Lei Wang, Duo Chen and Xinkui Fang contributed to perform experiments. ACE2-mouse animal model: Feng Li, En Zhang and Xiaoxiao Zhang. Analysis and interpretation of data: Yong Ke and En Zhang. Statistical analysis and drafting of the manuscript: Yong Ke and En Zhang. Critical revision of the manuscript: Tao sun, Jianwei Zhu and Baohong Zhang. Final approval of the manuscript: Tao sun and Baohong Zhang.

Conflicts of interest

The authors declare no competing interests.

Appendix A. Supporting information

Supporting data to this article can be found online at https://doi.org/10.1016/j.apsb.2023.08.023.

References

1. WHO. Coronavirus (COVID-19) dashboard. Available from: covid19.who.int.
2. Hatmal MM, Alshaer W, Al-Hatamleh MAI, Hatmal M, Smadi O, Taha MO, et al. Comprehensive structural and molecular comparison of Spike proteins of SARS-CoV-2, SARS-CoV and MERS-CoV, and their interactions with ACE2. *Cells* 2020;**9**:2638.
3. Bian J, Li Z. Angiotensin-converting enzyme 2 (ACE2): SARS-CoV-2 receptor and RAS modulator. *Acta Pharm Sin B* 2021;**11**:1−12.
4. Braun J, Loyal L, Frentsch M, Wendisch D, Georg P, Kurth F, et al. SARS-CoV-2-reactive T cells in healthy donors and patients with COVID-19. *Nature* 2020;**587**:270−4.
5. Chen Z, Du R, Galvan Achi JM, Rong L, Cui Q. SARS-CoV-2 cell entry and targeted antiviral development. *Acta Pharm Sin B* 2021;**11**:3879−88.
6. Awadasseid A, Wu Y, Tanaka Y, Zhang W. Current advances in the development of SARS-CoV-2 vaccines. *Int J Biol Sci* 2021;**17**:8−19.
7. Padron-Regalado E. Vaccines for SARS-CoV-2: lessons from other coronavirus strains. *Infect Dis Ther* 2020;**9**:255−74.
8. Topol EJ. Messenger RNA vaccines against SARS-CoV-2. *Cell* 2021;**184**:1401.
9. Wu F, Luo S, Zhang Y, Ou Y, Wang H, Guo Z, et al. Single-shot AAV-vectored vaccine against SARS-CoV-2 with fast and long-lasting immunity. *Acta Pharm Sin B* 2023;**13**:2219−33.

10. Chavda VP, Patel AB, Vaghasiya DD. SARS-CoV-2 variants and vulnerability at the global level. *J Med Virol* 2022;**94**:2986−3005.
11. Bleier BS, Ramanathan Jr M, Lane AP. COVID-19 vaccines may not prevent nasal SARS-CoV-2 infection and asymptomatic transmission. *Otolaryngol Head Neck Surg* 2021;**164**:305−7.
12. Harvey WT, Carabelli AM, Jackson B, Gupta RK, Thomson EC, Harrison EM, et al. SARS-CoV-2 variants, spike mutations and immune escape. *Nat Rev Microbiol* 2021;**19**:409−24.
13. Mercado NB, Zahn R, Wegmann F, Loos C, Chandrashekar A, Yu J, et al. Single-shot Ad26 vaccine protects against SARS-CoV-2 in rhesus macaques. *Nature* 2020;**586**:583−8.
14. Amanna IJ, Slifka MK. Contributions of humoral and cellular immunity to vaccine-induced protection in humans. *Virology* 2011;**411**:206−15.
15. Li H, Zhang Y, Li D, Deng YQ, Xu H, Zhao C, et al. Enhanced protective immunity against SARS-CoV-2 elicited by a VSV vector expressing a chimeric spike protein. *Signal Transduct Targeted Ther* 2021;**6**:389.
16. Wong G, Mendoza EJ, Plummer FA, Gao GF, Kobinger GP, Qiu X. From bench to almost bedside: the long road to a licensed Ebola virus vaccine. *Expet Opin Biol Ther* 2018;**18**:159−73.
17. Madar-Balakirski N, Rosner A, Melamed S, Politi B, Steiner M, Tamir H, et al. Preliminary nonclinical safety and immunogenicity of an rVSV-ΔG-SARS-CoV-2-S vaccine in mice, hamsters, rabbits and pigs. *Arch Toxicol* 2022;**96**:859−75.
18. Espeseth AS, Yuan M, Citron M, Reiserova L, Morrow G, Wilson A, et al. Preclinical immunogenicity and efficacy of a candidate COVID-19 vaccine based on a vesicular stomatitis virus-SARS-CoV-2 chimera. *EBioMedicine* 2022;**82**:104203.
19. Morozov I, Monath TP, Meekins DA, Trujillo JD, Sunwoo SY, Urbaniak K, et al. High dose of vesicular stomatitis virus-vectored Ebola virus vaccine causes vesicular disease in swine without horizontal transmission. *Emerg Microb Infect* 2021;**10**:651−63.
20. Huttner A, Dayer JA, Yerly S, Combescure C, Auderset F, Desmeules J, et al. The effect of dose on the safety and immunogenicity of the VSV Ebola candidate vaccine: a randomised double-blind, placebo-controlled phase 1/2 trial. *Lancet Infect Dis* 2015;**15**:1156−66.
21. Agnandji ST, Huttner A, Zinser ME, Njuguna P, Dahlke C, Fernandes JF, et al. Phase 1 trials of rVSV Ebola vaccine in Africa and Europe. *N Engl J Med* 2016;**374**:1647−60.
22. Fang X, Qi B, Ma Y, Zhou X, Zhang S, Sun T. Assessment of a novel recombinant vesicular stomatitis virus with triple mutations in its matrix protein as a vaccine for pigs. *Vaccine* 2015;**33**:6268−76.
23. Bewley KR, Coombes NS, Gagnon L, McInroy L, Baker N, Shaik I, et al. Quantification of SARS-CoV-2 neutralizing antibody by wild-type plaque reduction neutralization, microneutralization and pseudotyped virus neutralization assays. *Nat Protoc* 2021;**16**:3114−40.
24. de Haan C, Haijema B, Boss D, Heuts F, Rottier P. Coronaviruses as vectors: stability of foreign gene expression. *J Virol* 2005;**79**:12742−51.
25. Zhao X, Zhang R, Qiao S, Wang X, Zhang W, Ruan W, et al. Omicron SARS-CoV-2 neutralization from inactivated and ZF2001 vaccines. *N Engl J Med* 2022;**387**:277−80.
26. Nie J, Li Q, Wu J, Zhao C, Hao H, Liu H, et al. Establishment and validation of a pseudovirus neutralization assay for SARS-CoV-2. *Emerg Microb Infect* 2020;**9**:680−6.
27. McBride CE, Li J, Machamer CE. The cytoplasmic tail of the severe acute respiratory syndrome coronavirus spike protein contains a novel endoplasmic reticulum retrieval signal that binds COPI and promotes interaction with membrane protein. *J Virol* 2007;**81**:2418−28.
28. Havranek KE, Jimenez AR, Acciani MD, Lay Mendoza MF, Reyes Ballista JM, Diaz DA, et al. SARS-CoV-2 Spike alterations enhance pseudoparticle titers and replication-competent VSV-SARS-CoV-2 virus. *Viruses* 2020;**12**:1465.
29. Baum A, Fulton BO, Wloga E, Copin R, Pascal KE, Russo V, et al. Antibody cocktail to SARS-CoV-2 spike protein prevents rapid mutational escape seen with individual antibodies. *Science* 2020;**369**:1014−8.
30. Ma H, Guo Y, Tang H, Tseng C-TK, Wang L, Zong H, et al. Broad ultra-potent neutralization of SARS-CoV-2 variants by monoclonal antibodies specific to the tip of RBD. *Cell Discovery* 2022;**8**:16.
31. Ma H, Tseng C-TK, Zong H, Liao Y, Ke Y, Tang H, et al. Efficient neutralization of SARS-CoV-2 omicron and other VOCs by a broad spectrum antibody 8G3. *bioRxiv* 2022. Available from: https://doi.org/10.1101/2022.02.25.482049.
32. Ke Y, Yu D, Zhang F, Gao J, Wang X, Fang X, et al. Recombinant vesicular stomatitis virus expressing the spike protein of genotype 2b porcine epidemic diarrhea virus: a platform for vaccine development against emerging epidemic isolates. *Virology* 2019;**533**:77−85.
33. Zhao H, Lu L, Peng Z, Chen LL, Meng X, Zhang C, et al. SARS-CoV-2 Omicron variant shows less efficient replication and fusion activity when compared with Delta variant in TMPRSS2-expressed cells. *Emerg Microb Infect* 2022;**11**:277−83.
34. Hammarstedt M, Ahlqvist J, Jacobson S, Garoff H, Fogdell-Hahn A. Purification of infectious human herpesvirus 6A virions and association of host cell proteins. *Virol J* 2007;**4**:101.
35. Sugita Y, Noda T, Sagara H, Kawaoka Y. Ultracentrifugation deforms unfixed influenza A virions. *J Gen Virol* 2011;**92**:2485−93.
36. Chauhan VS, Furr SR, Sterka Jr DG, Nelson DA, Moerdyk-Schauwecker M, Marriott I, et al. Vesicular stomatitis virus infects resident cells of the central nervous system and induces replication-dependent inflammatory responses. *Virology* 2010;**400**:187−96.
37. Islam S, Islam T, Islam MR. New coronavirus variants are creating more challenges to global healthcare system: a brief report on the current knowledge. *Clin Pathol* 2022;**15**:2632010x221075584.
38. Li C, Ye Z, Zhang AJ, Chan JF, Song W, Liu F, et al. Severe acute respiratory syndrome coronavirus 2 (SARS-CoV-2) infection by intranasal or intratesticular route induces testicular damage. *Clin Infect Dis* 2022;**75**:e974−90.
39. Han P, Li L, Liu S, Wang Q, Zhang D, Xu Z, et al. Receptor binding and complex structures of human ACE2 to spike RBD from omicron and delta SARS-CoV-2. *Cell* 2022;**185**:630−40.e10.
40. Corbett KS, Flynn B, Foulds KE, Francica JR, Boyoglu-Barnum S, Werner AP, et al. Evaluation of the mRNA-1273 vaccine against SARS-CoV-2 in nonhuman primates. *N Engl J Med* 2020;**383**:1544−55.
41. Zhang S, Liu Y, Wang X, Yang L, Li H, Wang Y, et al. SARS-CoV-2 binds platelet ACE2 to enhance thrombosis in COVID-19. *J Hematol Oncol* 2020;**13**:120.
42. Lei HY, Ding YH, Nie K, Dong YM, Xu JH, Yang ML, et al. Potential effects of SARS-CoV-2 on the gastrointestinal tract and liver. *Biomed Pharmacother* 2021;**133**:111064.
43. Xu L, Liu J, Lu M, Yang D, Zheng X. Liver injury during highly pathogenic human coronavirus infections. *Liver Int* 2020;**40**:998−1004.
44. Wang Y, Liu S, Liu H, Li W, Lin F, Jiang L, et al. SARS-CoV-2 infection of the liver directly contributes to hepatic impairment in patients with COVID-19. *J Hepatol* 2020;**73**:807−16.
45. Cines DB, Bussel JB. SARS-CoV-2 vaccine-induced immune thrombotic thrombocytopenia. *N Engl J Med* 2021;**384**:2254−6.
46. Schultz NH, Sørvoll IH, Michelsen AE, Munthe LA, Lund-Johansen F, Ahlen MT, et al. Thrombosis and thrombocytopenia after ChAdOx1 nCoV-19 vaccination. *N Engl J Med* 2021;**384**:2124−30.
47. Tang J, Zeng C, Cox TM, Li C, Son YM, Cheon IS, et al. Respiratory mucosal immunity against SARS-CoV-2 after mRNA vaccination. *Sci Immunol* 2022;**7**:eadd4853.
48. Robbins JA, Tait D, Huang Q, Dubey S, Crumley T, Cote J, et al. Safety and immunogenicity of intramuscular, single-dose V590 (rVSV-SARS-CoV-2 Vaccine) in healthy adults: results from a phase 1 randomised, double-blind, placebo-controlled, dose-ranging trial. *EBioMedicine* 2022;**82**:104138.
49. Nyberg T, Ferguson NM, Nash SG, Webster HH, Flaxman S, Andrews N, et al. Comparative analysis of the risks of hospitalisation and death associated with SARS-CoV-2 omicron (B.1.1.529) and delta (B.1.617.2) variants in England: a cohort study. *Lancet* 2022;**399**:1303−12.

50. Kumar S, Thambiraja TS, Karuppanan K, Subramaniam G. Omicron and Delta variant of SARS-CoV-2: a comparative computational study of spike protein. *J Med Virol* 2022;**94**:1641−9.
51. Ren SY, Wang WB, Gao RD, Zhou AM. Omicron variant (B.1.1.529) of SARS-CoV-2: mutation, infectivity, transmission, and vaccine resistance. *World J Clin Cases* 2022;**10**:1−11.
52. Suzuki R, Yamasoba D, Kimura I, Wang L, Kishimoto M, Ito J, et al. Attenuated fusogenicity and pathogenicity of SARS-CoV-2 Omicron variant. *Nature* 2022;**603**:700−5.
53. Willett BJ, Grove J, MacLean OA, Wilkie C, De Lorenzo G, Furnon W, et al. SARS-CoV-2 Omicron is an immune escape variant with an altered cell entry pathway. *Nat Microbiol* 2022;**7**:1161−79.
54. Stukalov A, Girault V, Grass V, Karayel O, Bergant V, Urban C, et al. Multilevel proteomics reveals host perturbations by SARS-CoV-2 and SARS-CoV. *Nature* 2021;**594**:246−52.
55. Lee E, Oh JE. Humoral immunity against SARS-CoV-2 and the impact on COVID-19 pathogenesis. *Mol Cell* 2021;**44**:392−400.